OBSERVATIONS ON CAVITATION BUBBLE COLLAPSE

Albert T. Ellis

OFFICE OF NAVAL RESEARCH
Contract N6onr-24420 (NR 062-059)

CALIFORNIA INSTITUTE OF TECHNOLOGY
HYDRODYNAMICS LABORATORY
Report No. 21-12

Department of the Navy
Office of Naval Research
Contract N6onr-24420 (NR 062-059)

OBSERVATIONS ON CAVITATION BUBBLE COLLAPSE

Albert T. Ellis

Hydrodynamics Laboratory
California Institute of Technology
Pasadena, California

Report No. 21-12
December 1952

Approved by:
M. S. Plesset

ABSTRACT

Experimental observations are made on collapsing cavitation bubbles. Bubbles generated by two different methods are studied. The first method consists of bubble generation and collapse by flow over a submerged body. This work is done in the High-Speed Water Tunnel of the Hydrodynamics Laboratory. Existing photographic equipment and experimental techniques are employed. The second method consists of bubble generation and collapse by variation of the hydrostatic pressure. Much improved time and space resolution of the collapse is obtained in the latter case by design and construction of a high-speed photographic system. Bubble collapse pictures are taken at 10^5 frames per sec and an effective exposure time of 5×10^{-8} sec. A magnification of eight diameters from object to image is attained. This equipment reveals new details of cavitation bubble collapse.

Numerical solutions of the spherical bubble collapse equations are compared with experimental results. A consistently longer collapse time is observed in all cases. Observed bubble asymmetries are shown to be caused by pressure gradients. A large degree of coupling is shown to exist between the radial motion and the translational motion of the bubble centroid. Bubble collapse is observed to be much less stable than bubble growth.

CONTENTS

I. INTRODUCTION

Cavitation is the occurrence of cavities of vapor or vapor and gas phase in a region of liquid phase. These cavities may be formed in various ways, but the essential requirement for cavitation is a region of liquid in which the absolute pressure is less than or equal to the vapor pressure of the liquid. Either temperature or pressure may be varied to realize this condition. Boiling is an example of the former procedure, while pressure variation due to flow is the most common example of the latter. A large number of methods are readily seen to be available for the generation of such cavities. Some of these are:

1. Pressure variation by flow over submerged bodies.
2. Pressure variation in vortex motion of the liquid.
3. Pressure variation induced by vibrating boundaries.
4. Direct variation of the hydrostatic pressure.
5. Temperature variation by heating of the liquid.

Method 1 is usually thought of when cavitation is mentioned. This fact follows from the practical importance of cavitation generated in this way. Damage to ship propellers, pumps, and turbines results from the collapse of cavities produced in this manner. Increased drag of bodies moving through liquids, and loss of efficiency in devices to produce liquid flow also result. Methods 1 and 4 are studied in the research to be presented here. Method 1 is employed for its direct bearing on problems concerning flow, and Method 4 is used in an attempt to reduce the number of variables in the problem.

For preliminary description of cavitating flow about submerged bodies it is convenient to define a dimensionless cavitation parameter by

$$K = \frac{P_\infty - P_v}{\rho V_\infty^2} ,$$

where P_∞ is the static pressure at a large distance from the body, P_v is the vapor pressure of the liquid corresponding to its temperature, ρ is the liquid density, V_∞ is the flow velocity assumed uniform at a large distance from the body. This parameter is in general use, but it should not be expected to provide more than a very approximate measure of similarity between different cavitation conditions. Its origin stems from the work of Thoma[1]* on cavitation in pumps.

The first important work of a more theoretical nature concerning the collapse of an individual cavity was done by Lord Rayleigh[2] in 1917. This work followed an earlier formulation of the problem by Besant[3] in 1859. It is of historical interest to repeat the statement of the problem here:

> "An infinite mass of homogeneous incompressible fluid acted upon by no forces is at rest, and a spherical portion of the fluid is suddenly annihilated; it is required to find the instantaneous alteration of pressure at any point of the mass, and the time in which the cavity will be filled up, the pressure at an infinite distance being supposed to remain constant."

The solution of this problem by Rayleigh revealed indirectly that the physical assumptions were not complete, since the solution to the problem formulated involved infinite velocities and pressures at the collapse point. However, it did provide a basis for the explanation of physical damage to solid boundaries by collapsing cavitation bubbles. One of the best early attempts to correlate theory with experiment was made by J. Ackeret[4] in 1930. Actual experiments with submerged

---

* Numbers in parentheses refer to bibliography.

bodies in flow were carried out, and spark photographs were taken. A theoretical treatment of compressibility effects and shock waves was also made. This work helped to show that the subject of cavitation bubble collapse was vastly more complicated than that assumed in the simple Rayleigh theory. It rapidly became apparent that the essential features of cavitation bubble collapse were the most intractable ones.

From the theoretical standpoint, the existence of essential singularities in the simple theory made a detailed knowledge of fluid properties under extreme physical conditions very important for proper formulation of a more exact theory. One of the most comprehensive theoretical surveys of the subject is the recent work by Gilmore[5] of the Hydrodynamics Laboratory. This unifies and extends previous work on the compressibility and viscosity effects.

From the experimental view, essential data on bubble collapse was practically nonexistent prior to the high-speed photographic work reported by Knapp and Hollander[6]. This work provided photographs at 2×10^4 frames per second and revealed that still higher picture rates would be needed. The reason for this need is the high velocities attained by the bubble boundaries.

The objectives of the present work were formulated from a point of view reached by consideration of the foregoing development of cavitation research. It is hoped that the motivation for the type of research to be described has been made apparent. It is of an exploratory nature, with much time and effort spent on the development of experimental techniques which are essential to adequate observation. The need in the field of cavitation research is felt to be a proper orientation of theoretical work in directions indicated by experimental findings.

II. CAVITATION OBSERVATION IN THE HIGH SPEED WATER TUNNEL

The Purpose of the Water Tunnel Observations

The initial phase of this research concerns itself with the observation of cavitation produced by local reduction of pressure due to flow over a submerged body. This is the mode of growth and collapse of vapor bubbles normally meant when one speaks of cavitation.

Like many other natural phenomena, macroscopic cavitation effects and appearance have long been familiar, but details have been lacking which are vital to the formulation of a quantitative theory. This has simply been due to the great difficulty in making observations.

Some of the first work done on the high-speed photography of cavitation was reported by Knapp and Hollander[6] and the basic features revealed in their work was further discussed and clarified by Plesset.[7] The work of these investigators indicated the need for further high-speed photographic observations, particularly if these observations could be made with increased definition and speed.

It was decided that water tunnel investigations would be made with the following objectives:

1. Use of more than one type of model profile in order to vary the pressure-time history of the cavitation bubbles.
2. Attempt to measure the pressure distributions over the submerged models more accurately.
3. Determine photographic procedure to show maximum detail of bubble shape.
4. Use of a larger range of flow velocities and pressures in order to vary the amplitude and average value of the pressure-time curve.

Procedure and Observations

It was decided that an assortment of model shapes should include the original 1.5-caliber ogive used by Knapp and Hollander as well as a "half body" and a family of ellipsoids. An ogive is merely a sharp nosed body of revolution whose profile is generated by two intersecting circular arcs (see Fig. 17). A half body is the shape assumed by a bounding streamline in the case of a simple source in a uniform flow. The ogive was known to be capable of producing large easily observable bubbles, and the half body and ellipsoids would have pressure fields more easily calculable. Preliminary observation indicated, however, that the ellipsoid shapes available did not produce satisfactory cavitation. This group was therefore discarded. The half body seemed more successful and was retained.

Results of pressure distribution tests on both models are shown in Fig. 17. The 1.5-caliber ogive distribution agrees well with the previous one used by Knapp and Hollander. The half-body distribution agrees with the calculated theoretical value within experimental error. There seems to be no marked variation in the pressure at flow velocities up to sixty feet per second.

The next step was to try different photographic arrangements. The apparatus set up for top lighting on the model is shown in Fig. 1. The General Radio camera in the foreground provides film speeds up to one hundred feet per second.

Figures 2 and 3 are examples of front lighting photography similar to that used by Knapp and Hollander. The picture rate in this example is 19,000 frames per second. This arrangement shows flattening

of the bubbles normal to the flow direction just before collapse, but it does give the impression that they are reasonably spherical during most of their history. However, close examination of the mid-growth portion of Fig. 3 indicates a rather hemispherical shape. Figure 2 is interesting because of the very small bubbles which appear to exist in the wake of the larger bubble, and which appear to travel downstream at a much reduced velocity. These are probably small enough to be influenced by the boundary layer, the thickness of which may be estimated by the Blasius formula to be of the order of 0.006 in. in this case.

Top lighting from two separate lamps is illustrated in Fig. 4. Unfortunately, no bubbles close to the surface happened to be observed. The two highlights do show the flattened shape of the off-surface bubble obtained.

Back lighting is used in Fig. 5. It confirms the supposition of the flattened hemispherical shape barely noticeable in Fig. 3, and also provides better boundary detail. The irregular character of the rebound is quite apparent, and in this photograph some indication of boundary layer interaction may also be apparent.

It was then attempted to establish whether surface bubbles really resemble flattened hemispheres. Higher magnification and much lower picture repetition rate yielded the photographs shown in Fig. 6. Examples of the two types of bubbles are shown here which were observed throughout this work. They are, namely, the off-surface flattened type, and the surface-flattened hemispherical type. Presumably, the off-surface bubbles are more likely to have a considerable air content, as the minimum pressure must occur on the boundary if perfect fluid theory may be taken here to be a reasonable approximation. The

large size attained by both types of bubbles indicates that their growth may have been initiated from an unusually large air nucleus. An air bubble just entering the field of view is hard to detect because of compression in the high pressure stagnation region. Many bubbles which pass at large distances from the model surface have been observed to neither expand nor contract. This observation is taken to be evidence that air bubbles are present. It may be remarked that these results indicate that at least some of the bubbles described by Knapp and Hollander[6] have excessive air content. It is felt that the line of intersection between the large bubble and the model surface is sufficiently well highlighted in Fig. 6 to refute the obvious possibility of it being a spherical bubble with only the top portion visible above the model edge.

With the decision that the silhouette type of photography was best suited for bubble measurements, it remained to make runs for actual data collection. The half-body form showed a difficulty, in that only the smaller off-surface bubbles appeared to collapse very well. The larger bubbles behaved mostly as shown in Fig. 7, failing to collapse at all within the range of observation. An inspection of the pressure distribution curves in Fig. 17 shows that a bubble has a longer time to grow to a large size in the negative pressure region of the 1.5-caliber ogive. Once it has attained its growth, the rate of positive increase of pressure is also more rapid in the case of the ogive. This latter is also conducive to a good collapse. In the case of the half body, if the bubble collapses at all, it tends to flatten out as shown in Fig. 18. Therefore, only the ogive was used extensively.

Figures 8, 9, and 10 show the result of runs keeping the flow

velocity constant at about forty feet per second. The cavitation parameter, K, was varied by changing the static pressure. One-half the maximum length of the bubble in the direction of flow was the characteristic length plotted as experimental curves in Fig. 13 under the title of "bubble radius". It may be observed that in general the bubbles become smaller and the collapse occupies less time as the cavitation parameter is increased at constant flow velocity. This result is to be expected. Figure 14 shows a collapse at the much higher velocity of eighty-five feet per second. The collapse is much more rapid due to the greatly increased amplitude of the pressure-time curve.

Theory of the Spherical Collapse

At this point it becomes necessary to outline the simple theory involved in the spherical collapse situation in order to better understand the presentation of data.

It is well realized by the author that the spherically symmetric problem may seem superficial in the light of the data already presented. However, it should be viewed as the best available first approximation, and license to be over critical is denied by the existence of many other considerations such as thermal effects, compressibility, and viscosity.[8]

Following Plesset,[7] one must extend Rayleigh's[2] solution for the collapse of a spherical cavity in a liquid with constant pressure at large distances from the cavity to the case where the pressure varies quite rapidly. Let the origin of coordinates be at the bubble center, which is at rest. Let the radius of the bubble be $R(t)$ and let r be the radius to any point in the liquid. The velocity potential under the spherically symmetric assumption may be written as[9]

$$\varphi = \frac{R^2 \dot{R}}{r} \quad . \tag{1}$$

The equation of motion in integral form becomes

$$-\frac{\partial \varphi}{\partial t} + \frac{1}{2}(\nabla \varphi)^2 + \frac{P(r)}{\rho} = \frac{P(t)}{\rho} \quad , \tag{2}$$

where $\dot{R} = \frac{dR}{dt}$, $P(r)$ is the static pressure at r, $P(t)$ is the static pressure at a distance from the bubble, and ρ is the liquid density. From Eq. (1),

$$(\nabla \varphi)^2 = \frac{R^4 \dot{R}^2}{r^4} \quad . \tag{3}$$

Applying Eq. (2) at $r = R$, one obtains the equation of motion for the bubble radius. Thus, with

$$\left(\frac{\partial \varphi}{\partial t}\right)_{r=R} = 2\dot{R}^2 + R\ddot{R} \quad , \tag{4}$$

$$(\nabla \varphi)^2_{r=R} = \dot{R}^2 \quad ,$$

and Eq. (2) yields the motion of the spherical bubble boundary

$$R\ddot{R} + \frac{3}{2}\dot{R}^2 = \frac{P(R) - P(t)}{\rho} \quad , \tag{5}$$

where $P(R)$ is the pressure in the liquid at the bubble boundary. In the water tunnel work, the assumption is made that the pressure inside the cavity is the vapor pressure, P_v, of the liquid at the bulk temperature. Hence, if surface tension is included,

$$P(R) = P_v - \frac{2\sigma}{R} \quad , \tag{6}$$

where σ is the surface tension constant for water at the appropriate temperature. The function, P(t), is determined from the noncavitating pressure distribution over the body plus photographic record of the position of the bubble relative to the body profile as a function of time. When P(t) is obtained, the integration of Eq. (5) may be carried out to get the radius of the bubble as a function of time. The integration was performed numerically. The solution is determined when two constants are specified, and these were taken to be the observed value of the maximum radius where the radial velocity is zero.

Comparison of Experiment with Theory

It is apparent that the most outstanding failure of the simple theory is to account for the twenty or twenty-five percent greater collapse time observed. This finding supports that originally made by Plesset.[7] These bubbles are seen to grow from small proportions to full size in a time so short as to prohibit significant air diffusion across the interface[10] but, as previously mentioned, an air nucleus might have existed all the time. An excessively large air content would account for the longer collapse time.

Another explanation of the increased collapse time was presented by Rattray[11] who calculated the effect of rigid boundary proximity on the collapse. His calculations showed about a twenty percent increase in collapse time. This prediction gives approximately the right value to explain the discrepancy.

It should be pointed out, however, that Rattray assumed an initially spherical bubble collapsing near a wall. The observations in this work indicate that at least the larger bubbles, similar to those measured, are more like hemispheres. It is obvious from considerations of

symmetry that if the bubbles were indeed hemispheres, and if viscous and surface tension effects at the rigid boundary were neglected, then the bubble should collapse in the same manner as in the spherical case away from all boundaries. The collapse time observed, of course, does not agree with this latter concept. It is mentioned here only to lend support to the possibility of other effects contributing to this increased collapse time.

The Contribution of Pressure Gradients to Bubble Asymmetry

It has been pointed out by Plesset[7] that one approximation in the spherical theory consists in neglecting pressure gradients both along the model surface and normal to it. In the light of observed bubble asymmetry, it seems worthwhile to calculate some of these pressure gradients to see if the pressure change really is small over a distance of the order of a bubble diameter. This calculation would involve a prohibitive amount of computation for the ogive shape, but fortunately it is less difficult for the half body, and this simplicity was, of course, one reason for choosing the latter shape. It is also not markedly different from the ogive, so that the general behavior of the two pressure fields should be similar.

The pressure field of the half body was computed and plotted in Fig. 16. For easy visualization, a dashed line is drawn in to show the approximate path of a particular collapsing bubble photographed in Fig. 15 on the opposite page. The manner in which the flat on the bubble rotates to maintain itself parallel to the lines of constant pressure in the field is quite evident. This behavior is found in spite of the fact that the bubble shown is relatively small (about 0.05 in. maximum radius) and hence should be less affected by space gradients in the pressure.

It is further to be noted that the flat is on the side of the bubble next to the higher pressure region. This behavior is similar to that found for a bubble collapsing in a hydrostatic pressure gradient. Here, also, the flat appears on the bottom, which is the side of greatest pressure. (See spark generated bubble in Fig. 26.)

It is also clear that space gradients in the pressure will increase with increased flow velocity. These effects should then become more apparent. That this is true may be seen by comparing the bubble asymmetries in Fig. 11 with those in Figs. 8 and 9. The former seems more affected at eighty-five feet per second than do the latter two at forty feet per second. It should also be noticed that the small off-surface bubble in Fig. 12 develops a flat at the same angle as does the larger surface bubble in Fig. 11 for similar positions along the model profile.

In view of these observations, it seems not unlikely that pressure gradients may be a dominant factor in determining bubble histories. Even small bubbles might be affected since the small bubbles in fine grained cavitation are found where the pressure gradients are large. Pressure gradients are certainly important in situations such as shown in Fig. 20. Apparently the cavity here has almost succeeded in maintaining itself or making the transition to the third regime of flow from the second.[7]

Nonrebound of the Bubble

Figure 19 is an example of the rather rare occurrence of collapse without rebound. Instances of this are also to be found in later parts of this thesis, but it is believed that this is the first time an example has been observed in the High Speed Water Tunnel.

It is felt that absence of rebound characterizes the collapse of bubbles free of permanent gas. Theoretical considerations at present indicate that the tensile strength of water is sufficient to prevent the short-duration dilatation wave following the collapse from reopening the cavity. The fact that such behavior is rarely observed is largely a measure of the difficulty of obtaining water in the working section of the water tunnel free of air bubbles. Since a permanent gas is compressed adiabatically during the very rapid collapse, the partial pressure in the cavity due to this permanent gas will be extremely high for small values of the radius, and this internal pressure will prevent closure. It might be argued that the apparent rarity of occurrence of nonrebound bubbles makes this type of less practical importance. This argument should be viewed with great caution since the less frequent occurrence of nonrebounding bubbles may be a characteristic of the limited types of observations on cavitation bubbles which are available at present. The observational techniques developed in this research will make possible observations on small nonrebounding bubbles with their very short lifetimes. When this type of cavitation bubble can be conveniently generated in the laboratory, they will be accessible to photographic study and the cavitation damage problem may then be more effectively attacked.

III. EXPERIMENTS WITH COLLAPSING GLASS SPHERES

Purpose and Procedure

At the suggestion of Professor Plesset it was decided to investigate the possibility of collapsing thin glass spheres under hydrostatic pressure. If feasible, this method of investigating collapse would make it possible to use various initial cavity contents. One could start with a vacuum and then progress to various vapors and permanent gases.

The success of such an experiment obviously depends on how well the glass sphere shatters. It was found impossible to procure special shatter glass sufficiently thin and in spherical form. Ordinary soft glass was then tried, but the results were unsatisfactory, and the experiment was discontinued. If the technical difficulty with the glass could be solved, it would prove a useful avenue of investigation.

The apparatus is shown in Fig. 21, and typical results are illustrated in Figs. 22 and 23.

IV. DEVELOPMENT OF THE HIGH-SPEED PHOTOGRAPHIC SYSTEM

Consideration of Requirements

The photographic equipment and technique developed in this thesis research is such as to meet the requirements for cavitation observation with a minimum of expense and effort. No attempt was made to arrive at an optimum design whenever this appeared nonessential for obtaining satisfactory information on the immediate problem. The minimum requirements set up, however, proved to be quite stringent in terms of the present status of high-speed photography. As a consequence, the major portion of time spent in this research was devoted to this rather extraneous but absolutely necessary problem.

Water tunnel cavitation experiments indicate that an increase of at least an order of magnitude is needed both in time and space resolution of the bubble radius-time record. Photographic repetition rates of the order of 200,000 pictures per second with bubble radii measurements accurate to about 0.001 in. are desired. A sufficient number of such pictures must also be taken to cover adequately the bubble collapse history, which is usually an interval of from one to two milliseconds.

A survey of the literature failed to disclose that any system had been reported which was capable of meeting all of these requirements, and such systems that showed promise for adaption appeared to require mechanical or optical design and construction work far exceeding available time and finances.

Several high-speed cameras using optical or mechanical shuttering methods were reported which were capable of the desired picture

repetition rate, but the exposure times employed were too long for this application. As an example, one might mention the type suggested by Professor I. S. Bowen,[12] a prototype of which attained repetition rates of the order of 4×10^5 per second but employed an exposure time of about one microsecond. A general survey of high-speed photographic systems of this and other types is to be found in the literature[13] and will not be discussed here.

In most high-speed cameras, maximum exposure time is determined by considerations of frame size and repetition rate, as these factors determine the effective scanning or film speed. However, in the case of very small objects moving with high velocities, such as cavitation bubbles, blurring of the image occurs from movement of the object itself, which is an effect in addition to blurring caused by high film or scanning speeds. The latter may be removed or reduced by optical compensation methods which eliminate relative motion between film and image during the exposure time. The former obviously cannot be eliminated in this manner and hence exposure time must be shortened.

In the cavitation problem, for example, if the magnification is 10 and the bubble wall velocity is 10^3 in. per sec., then to keep the bubble measurement accurate to 10^{-3} in. requires maximum exposure times of the order of 10^{-7} sec. On the other hand, an equivalent blurring due to uncompensated relative motion between image and film of 4×10^4 in. per sec. would, at the same magnification, require a maximum exposure time of 2.5×10^{-7} sec. These figures are representative of conditions existing in the present work, and thus bubble wall velocity is seen to be the dominant factor in setting the rigid requirement for short exposure time.

It should be mentioned here that the "streak" camera providing a record of variation of one linear dimension only and requiring no shutter at all might have been feasible had the bubble remained spherically symmetrical. In light of the present work, however, it is clear that such data would have been quite useless.

The two major problems therefore resolved themselves into that of finding a light shutter of very short duration and high repetition rate, together with a source of illumination intense enough to provide adequate film exposure at such high magnification and short intervals. It was realized from the start that the lesser problem of providing image transport over the film at speeds of the order of 4×10^4 in. per sec. could be solved by a rotating mirror or prism method, and that motion of the film itself at such speeds would be impractical.

The Light Shutter

A Kerr cell electro-optical shutter appeared capable of meeting exposure time requirements.[14] Figure 27 shows the Kerr cell used in this work. This type of shutter has long been well known, consisting merely of two light polarizers (such as Nicol prisms or the more modern polaroid film) on either side of a cell containing a substance such as nitrobenzene in a controlled electric field. The polarizers are adjusted so that a minimum of light passes through them and the nitrobenzene when the electric field is off. Upon application of the field, the nitrobenzene causes an additional rotation of the plane of polarization so that the light is then transmitted through the second polarizer. The speed of operation of the Kerr cell is limited in practice only by the speed at which the electric field can be applied and removed. The

disadvantages of the Kerr cell are that there is only about twenty percent transmission of light when it is full open, and the nitrobenzene further acts as a light filter to cut off the blue end of the spectrum which is most effective for many film emulsions. For a practical size of cell the electric potential required is about 13,000 volts, and this voltage makes design of a pulser a major electronic problem. It is also liable to produce optical distortions if an image is passed through it with too widely divergent rays, or if convection currents in the fluid are set up by the applied electric potential. These latter effects are exaggerated if impurities exist in the nitrobenzine or in the nickel electrodes.(15)

In spite of these difficulties, however, A. M. Zarem and F. R. Marshall(16) have recently photographed self luminous objects such as exploding wires by means of a number of Kerr cells, each having an electric pulse of very short duration (0.04 microsecond effective exposure time) applied to it by an independent electrical circuit. In this manner a series of three pictures was taken, separated by arbitrarily short intervals. This technique is quite effective if only a very small number of consecutive pictures are required, but it is obviously impractical for a study of cavitation where at least several hundred pictures should be obtained to cover adequately the required time interval. This latter consideration very greatly increases the difficulty of the problem, especially in regard to electronic design of a suitable pulser. It also introduces the problem of image transport, as a conventional plate camera such as used by Zarem and Marshall could not accommodate many exposures.

From these considerations it became clear that a new approach

to the problem was necessary. The method decided upon was to use a single Kerr cell in conjunction with electronic equipment which would apply a series of electric pulses of proper duration at the desired repetition rate. Also, since bubbles are nonluminous, a suitable light source was required, and it appeared possible to circumvent optical problems involved in passing an image through the Kerr cell by merely using it to shutter the illumination. The Kerr cell with its pulser and a light source would then in effect become a "stroboscopic light" rather than an integral part of the camera. This procedure has the advantage of permitting extremely simple camera design with better image definition. Its disadvantage lies in the fact that for small aperture Kerr cells (the aperture of the one used was three-eighths of an inch), a very intense light source is required, and the illumined field is rather small.

The Light Source

A very great amount of time and effort was spent in obtaining a light source of sufficient intensity to give normal exposure to fine grain film (panatomic X) at magnifications of about ten and an exposure time of less than one-tenth microsecond.

The first source tried consisted merely of a No. 50 flash bulb, and this gave quite useable exposures. Unfortunately, it could not be used because of the delay time of thirty milliseconds before reaching peak intensity. It was estimated that only about five milliseconds were required for the bubble to grow to excessive size, and the only available flash bulb having such a short delay time was the SM type which was of insufficient intensity.

A high pressure mercury arc was then tried as a light source which would be left on continuously. This consisted of a General

Electric type AH-6 water cooled lamp operating at one thousand watts direct current input. This did not provide sufficient light, and an attempt was made to raise the intensity by pulsing the lamp in a manner similar to that employed at the Ames Aeronautical Laboratory.[17] Although sufficient intensity was believed to have been obtained, the arc was too unstable under pulsing conditions to permit reliable operation, and hence this system was discarded.

It was felt at this time that any suitable lamp would require such magnitude of input energy that only by pulsing it at the picture repetition rate could the heat dissipation be kept within allowable limits. Consequently, work was started by the electronics group of the Hydrodynamics Laboratory on pulsing equipment using hydrogen thyratron tubes similar to their existing equipment but capable of much higher repetition rates. As the success of this undertaking could not be foreseen, parallel work was started by the author on a hard vacuum tube system. The final amplifier in the latter system employed a pair of Type 527 radar modulator tubes operated at 20,000 volts plate potential with pulse currents of 100 amp each. This amplifier is shown in Fig. 28. A special pulse transformer was constructed using a one-square-inch hypersil core in an attempt to provide a better impedance match to the low resistance flash lamps used. However, only about 300 amperes current to the flash lamp was obtained, while the hydrogen thyratron unit proved to be quite successful in delivering several times this current. The thyratron unit was found to be quite reliable for pulsing the standard Edgerton flash lamps at 100,000 pulses per sec. and about 0.3 joules per flash. This represented a considerable accomplishment by Mr. Haskell Shapiro and his group, as nothing approaching this performance had

been accomplished previously.

It was hoped that this development would permit the use of a short duration flash tube such as the General Electric FT-230 without any Kerr cell at all. Subsequent tests revealed that the FT-230 had a high intensity flash for about 0.2 microsecond, followed by a rather long afterglow which became more noticeable as the repetition rate was increased. Several bubble pictures were taken with this equipment, but the photographic quality was rather poor. An example of such a picture is given in Fig. 29. A picture of a bead of solder taken with the standard FT-25 flash lamp is shown in Fig. 30. This lamp has a normal flash duration of about 1.5 microseconds. The outlines are hardly distinguishable at all, but it should be noted that the film scanning speed used was 3,200 feet per sec, or 32 times that of the General Radio high-speed camera normally used with these lamps.

These tests indicated that no flash lamp was available which could be used directly without employing a Kerr cell to limit the light duration, although the General Electric FT-230 or FT-231 comes nearest to meeting the requirements. They might prove satisfactory for exposures of the order of 0.2 microsecond providing the long afterglow or "tail" were minimized by "stopping down" the camera. This opinion was strengthened by a discussion of the matter with Professor Germeshausen of Massachusetts Institute of Technology, who, in association with Professor Edgerton, has long been a pioneer in gaseous discharge and flash tube development. Professor Germeshausen felt that the development of high intensity flash lamps of less than about 0.5 microsecond flash duration had become a matter of diminishing returns.

Means were therefore taken to synchronize the lamp pulser with

the Kerr cell pulser in order to shorten the flash from the FT-231. This synchronization was made rather difficult by failure of the hydrogen thyratrons in the lamp pulser to fire at exactly equal intervals. This time "jitter" required that the Ker cell pulse be initiated directly by the flash lamp pulse, rather than by the exiting pulse to the grids of the thyratrons. In order to prevent the lamp from firing before the Kerr cell opened, it was necessary to delay the flash by connecting the lamp to the end of about thirty feet of coaxial cable which served as a delay line.

The above mentioned arrangement gave very sharp but somewhat underexposed pictures. The amount of electronic equipment involved had grown to rather ponderous proportions, however, and it was decided to reexamine the possibility of obtaining a light source which could remain on during the entire observation period. It had been noticed by the author that a new flash lamp manufactured by General Electric had characteristics which made it quite suitable for this purpose. This lamp was the GE 524. It had an input rating of 2×10^3 joules per flash for a flash duration of about one-half millisecond, which is equivalent to an input of 4×10^6 watts. The peak light output rating was 10^8 lumens. This rating inspired great confidence in the possibility of solving the illumination problem, since previous experience had shown that the number 50 flash bulb gave mediocre results with a peak rating of only 5×10^6 lumens. Both sources are of approximately the same physical size. In order to spread the 524 flash over the required two milliseconds instead of the rated one-half millisecond, it was felt to be necessary to reduce the light output to about 25×10^6 lumens. This output would still provide a comfortable margin in the illumination.

The 524 lamp proved capable of meeting all expectations, and therefore it was the source adopted for this work. A photograph of this lamp is shown in Fig. 31. It is a quartz helix filled with Xenon gas at rather low pressure. The operating voltage may be in the range of two to four thousand volts, but a ten to fifteen thousand volt triggering pulse is required.

The only remaining technical problem in connection with the light source was that of lengthening the electrical pulse to cover the required two-millisecond observation time. This lengthening was facilitated by the fact that the lamp impedance is about four or five ohms. This impedence is considerably more than that of most flash lamps, and it permits the required energy to be stored in an electrical network resembling a lumped parameter delay line or filter with reasonable values for the inductances and capacitances involved.[18] M derived sections with inductive coupling between sections were used in an attempt to obtain a nearly rectangular current waveform to the lamp. This type of waveform is obviously preferable since the illumination would then remain constant. Normal practice with the Type 524 lamp is to use a simple inductance and capacity combination which results in a beehive shape of current waveform. This waveform would be quite undesirable for the present purpose. Resistance elements for lengthening the discharge are impractical because of the large energy loss which would be necessary. The waveform actually attained was quite acceptable but left something to be desired. It is almost impossible to calculate the circuit constants correctly because the lamp behaves as a nonlinear circuit element during a portion of the discharge. The storage network in its aluminum housing may be seen at the extreme left in Fig. 32. The rather large physical

size is due to the condenser bank consisting of 240 microfarads at 4,000 volts rating. The inductances are small (1.14 millihenries) and may be seen lying on top of the housing.

The Camera

The rather simple camera arrangement may be seen in Figs. 35, 36, and 37. Since film scanning speeds of the order of 3,000 feet per sec. were required, it was thought impractical to move the film. Instead, a rotating mirror was employed to move the image relative to the film. A very important requirement also was that the camera be ready to take pictures at any instant since the vapor bubbles occur at random. For these reasons, the camera was constructed so that the film would lie in the form of a circle, emulsion side inwards. At the center of the circle a rotating mirror was mounted with its surface making an angle of forty-five degrees with the axis of rotation. The camera lens was also mounted on the axis of rotation such that the image rays would be reflected by the rotating mirror and focus on the 35 mm. film along the circular periphery. This arrangement has the disadvantage that the image appears to rotate 360 degrees for each complete revolution of the mirror, but this is inconsequential for obtaining data. This feature could be corrected by use of a rotating prism if pictures were desired for direct reprojection. It should be mentioned here that arrangements wherein the mirror axis of rotation is perpendicular to the incoming rays from the lens are capable of twice the angular scanning velocity attainable with the arrangement used here. They are generally more subject to optical errors, however, and for a complete analysis of these the literature should be consulted.[19]

An f 1.5 lens of 3 inches focal length is used at present, giving an over-all magnification of about five. Well exposed pictures have been obtained at magnifications of about ten, however. At its present crude stage the camera must be loaded in darkness, and the film is held in place by a simple retainer ring. The arrangement is shown in Fig. 37. The circumference of the film track is 90 in. The rotating mirror is driven by a small direct current motor at speeds up to 25,000 rpm. The present mirror presents an aperture of 1 in., which is insufficient to avoid the loss of a considerable amount of light. However, this latter has imposed no particular hardship with the intense light source used.

Much revision of the camera design is planned in the near future. With the exception of excessive frame overlapping at 100,000 frames per sec, the present version has sufficed to obtain data, which has been the only immediate concern. This frame overlapping is due to the inadequate speed of the rotating mirror, which moves the image about three-eighths of an inch at this repetition rate. An air motor drive has already been procured which will increase the angular speed by a factor of four. It is anticipated that the correspondingly shorter observation time will still be sufficient for the studies contemplated, but it seems quite possible to adapt the camera to accommodate longer film lengths if this proves desirable.

The Pulse Generator for the Kerr Cell

Design of the Kerr cell pulser proved to be one of the major problems in this research. The fundamental difficulty is that a rectangular shaped voltage pulse of 13,000 volts magnitude and 0.1 microsecond duration is required at the desired picture repetition rate. To make

matters more difficult, the voltage must be delivered to a Kerr cell which electrically resembles a capacitance of 50 to 100 micro-micro-farads. About 26 amp output current is therefore required for a voltage rise rate of 2.6×10^{11} volts per sec, corresponding to 0.05 microsecond duration slopes on the pulse edges.

Kerr cell work, which is known to have been done to date, appears to fall into two categories. The first resembles that of Zarem and Marshall[16] in which single pulses of short duration (of the order of 0.05 microsecond) are applied to the Kerr cell, and the second is like that of Bowersox[20] in which relatively long (1.0 microsecond) pulses are applied at relatively low (12,500 per sec) repetition rates. Of course, in both of these systems, as in any other, the repetition rate may be effectively increased merely by increasing the number of Kerr cells employed. In addition to increasing the amount of equipment required, this method introduces complications in the optical system and camera in order to preserve similarity between the images from the different cells and to provide proper synchronization. However, such a procedure seems justified on the basis that it effectively multiplies the capabilities of a given system.

For the single pulse type of generator, the circuits used by Zarem and Marshall[16] seem rather simple and effective, and the reader is referred to their paper. Basically, they employ a hydrogen thyratron, the ionization of which provides the rapid voltage rise required. The waveform of this pulse is not directly suitable for operation of the Kerr cell, and hence an output circuit network employing inductance, capacitance, and resistance is required in order to shape the pulse. For high repetition rates, however, the thyratron tubes are impractical

because of the deionization times required, particularly at such high potentials. Much experience with these tubes for pulsing Edgerton type flash lamps indicates that special precautions must be taken when operating at repetition rates greater than 5,000 per sec.

Hard vacuum tubes, on the other hand, do not suffer from these "hold over" troubles, but the problem of getting high voltage rise rates and high output currents is more difficult than with the gaseous thyratron tubes. Much work of this type was done on radar pulse modulators during the war, but here again the repetition rates were usually much less than 10,000 per sec and the pulse durations longer than a microsecond.(21)

In view of these facts, initial work on the pulse generator consisted in trying to increase the repetition frequency of a hydrogen thyratron (Type 4c35) in a "line charging" circuit similar to those developed for radar purposes. This procedure was suggested by Mr. H. Shapiro, and the mode of attack on the problem consisted of lowering the anode potential and lowering the impedance in the grid circuit. It was found that high voltage pulses could not be obtained, but satisfactory pulses of about 250 volts amplitude were possible at a repetition rate of more than 200,000 pulses per sec. This performance seemed to give a quite satisfactory generator at the time, provided high vacuum tubes could be employed as amplifiers to raise the pulse voltage. Further use revealed this generator to be rather erratic, however, and only certain particular thyratrons would deionize properly. Fortunately, it was realized by the author about this time that a commercially available square wave generator manufactured by Tektronix, Incorporated, was capable of delivering a square wave with 0.02 microsecond rise time into a 50 ohm load. This

performance seemed ideal for the present purpose if it could be adapted to the generation of short pulses instead of square waves. A simple solution to this problem was conceived by the author which proved very satisfactory in practice. It consisted merely in delaying the square wave by letting it propagate down a 50-ohm coaxial cable and then subtracting this delayed square wave from the original one. It is plain that the result will be a series of alternately positive and negative rectangular pulses of the desired form. The length of these pulses is then proportional to the length of the cable and quite independent of the repetition rate. The voltage rise rate is preserved quite well, and the waveform is good when the coaxial line is properly terminated in its characteristic impedance.

The functions of the circuits following this pulse-forming stage should be obvious from the diagram shown in Fig. 39. A few comments on the design may be helpful, however. It should be noted that the 5687 tube in the pulse-forming stage is a recent type having a very large transconductance and low plate resistance. Used with a plate load resistance of only 900 ohms, it does not increase the rise time appreciably although it might be advisable to decrease this resistance still further if it is desired to keep the pulser rise time very close to 0.02 microsecond. The same comment applies to the plate loads in the subsequent stages. This low plate resistance requirement makes it necessary to employ at least two 715C output tubes. The pulse current is of the order of 20 amperes. If it proves desirable to go to still shorter exposure times and higher repetition rates, the high power amplifier already constructed and used as a light source pulser may be used. It will supply pulses of 200 amps at about 16,000 volts. In view of this, Kerr cells of much larger aperture

and correspondingly greater capacitance may be feasible. The use of low load resistance in the final amplifier also eliminates the need for any pulse shape correcting network at this point and preserves the form obtained in the low power level stages. In this connection it should be emphasized that the input pulse transformer to the final amplifier must have few turns and a large hypersil core to minimize pulse distortion. This transformer was used for phase reversal in order that both the final amplifier and its driving stage may be in the nonconducting state except during the transmission of a pulse. This behavior is required in order to avoid prohibitive power dissipation.

The circuit constants chosen provided satisfactory operation at the repetition rates and observation times required. The large current requirements were met by means of condenser storage. The pulser apparently operated satisfactorily at a repetition rate of 10^6 per sec and an electrical output pulse duration of about 0.1 microsecond. At this repetition rate the pulse magnitude dropped rapidly, however, because of insufficient storage capacitance in the power supplies.

Although considerable care was employed to insure rapid voltage rise rates in the electrical pulse to the Kerr cell, it should be mentioned that this requirement is rendered less severe by the light transmission characteristics of the Kerr cell itself. As pointed out by Zarem and Marshall,[16] the transmission, T, of axial rays is given by

$$T = A \sin^2 \left[\frac{\pi}{2} \left(\frac{v}{V} \right)^2 \right] ,$$

where v is the voltage applied to the electrodes, V is the "full open" voltage of the cell, and A is a constant which takes into account rejection of one-half of the light by the first polarizer and absorption and

reflection losses in all components of the shutter. As a result of the relation given, it turns out that the minimum effective exposure time attainable with a given pulser is slightly less than one half of the rise time of the electric pulse.

It is estimated that the over-all rise time of the pulser developed in this thesis research is about 0.04 microsecond. Minimum effective exposure times of 0.02 microsecond at a repetition rate of 10^6 per sec are therefore available.

Photographs of this equipment are shown in Figs. 33 and 34.

Suggested Future Applications of the Photographic Technique

Many applications of this high-speed photography immediately suggest themselves, but it should be particularly pointed out that the light from a Kerr cell shuttered source is polarized. This minimizes further loss of light in applications where polarized light is required. Such applications include studies of propagation of transient stresses in photoelastic models and transient behavior of shock waves in fluids. Other uses not necessarily requiring polarized light include ballistics studies and underwater explosions. These applications are in addition to the Hydrodynamic Laboratory's own interest in future cavitation and cavitation damage work.

Professor Lindvall has suggested investigation of applicability to the study of certain chemical reactions where phase transition observations are desirable. These include combustion and many others.

Professor Wiersma has suggested study of nerve fibres to determine what physical changes occur during transmission of a nerve impulse. These latter applications utilize the magnification capabilities of the system.

V. COLLAPSE OF VAPOR BUBBLES IN THE ABSENCE OF FLOW

The Purpose of the Observations

The preceding work in the High-Speed Water Tunnel revealed that there were many factors affecting cavitation bubble collapse. These included pressure gradients due to flow, the proximity of the model surface to the collapsing bubble, and the presence of air nuclei of unknown size. There is also nearly always some uncertainty introduced by the boundary layer and by turbulence whenever flow is involved. It was, therefore, thought desirable to attempt to eliminate some of these factors and to provide experimental conditions more favorable for analysis of bubble collapse. The technique of generating vapor bubbles by boiling at reduced pressure and then increasing the pressure to cause collapse seemed to provide a means of producing bubbles in stationary liquid. It was obvious that the procedure introduced timing difficulties, but for very high-speed photography the timing problem is present in any case. If, in addition, detection of bubbles formed in the center of the fluid could be effected, then proximity of solid boundaries would be eliminated. Although these disturbing factors may always be present in cavitation of practical interest, little progress in solving the problem is likely unless the number of variables is reduced for a first approximation.

Technique and Apparatus

To form vapor bubbles by boiling, it is necessary to lower the pressure or increase the temperature, or both. Care must be taken to use clean containers and uniform heating if bubbles are to be formed at random away from boundaries. To observe collapse of random bubbles it is also necessary to wait until a bubble happens to form in the field of

view and then to collapse it by applying pressure rapidly enough so that the bubble does not grow too large before collapse begins. The frequency of bubble formation is determined by the number of possible nuclei present for the same conditions of pressure and temperature. Using air-saturated distilled water and limiting the boiling to a value where turbulence was low gave a bubble formation frequency of about once every three or four minutes in a one-eighth inch field of view. Since the observation time covered by the camera is only two milliseconds, it is obvious that a bubble detector is essential. This detector must not only start the photography at the proper time, but it must also apply pressure to the liquid to initiate collapse. Such a detector was constructed using a pair of type 931-A electron multiplier photocells. A narrow light beam was directed up through the center of the glass container for the fluid. The field of observation of each photocell was limited by an aperture and lens to a small segment of this vertical beam which was also in the field of view of the camera lens. Thus, if a bubble formed in this region of the light beam, it would scatter light to the two photocells. The photocells were connected in a coincidence circuit such as is commonly used in nuclear counting arrangements. By this method both cells must receive light from the bubble at the same time. This arrangement prevents triggering on very large bubbles or on reflections from the surface. The bubble detector chassis may be seen on top of the smaller rack in Fig. 34. The two photocell housings are shown in Fig. 35, and the large cylindrical housing for the bubble detector light source and condensing lenses is just below the pyrex glass liquid container.

The cycle of operation is best described by referring to the block diagram in Fig. 40. When the camera motor is up to speed, the camera

lens cover is removed and the bubble detector placed in operating condition. The restriction between the liquid container and the vacuum pump is adjusted until the pressure drops sufficiently below the liquid vapor pressure for bubbles to form. When a bubble trips the detector, a hydrogen thyratron is triggered which discharges a 130 microfarad condenser charged to 1100 volts through a solenoid type air valve. This discharge operates the valve within 0.005 second and allows atmospheric air pressure to enter the fluid container to collapse the bubble. When the pressure starts to rise, it does so nearly linearly with time, taking a minimum of about 0.0015 second to reach equilibrium when the container is nearly full of liquid. The air flow through the restriction is always negligible compared to the flow through the solenoid valve and hence does not limit the rate of pressure increase in the container. The usual procedure consists in boiling the water at about one-tenth atmosphere and then causing bubble collapse by raising the pressure to one atmosphere. At the same time that the bubble detector activates the solenoid valve, it also sends a signal through a time delay unit. This unit allows time for the pressure to begin to rise in the liquid container, and then it starts the Kerr cell pulser and pulses the light source simultaneously. The Kerr cell is pulsed during the interval that the light is on. This interval is equal to or less than the period of one revolution of the camera mirror so that there is no overlap of images on the film. The purpose of the lens between the Kerr cell and the liquid container is to focus the illumination at the point in the liquid where a bubble will actuate the detector. The lens field also serves to provide framing for each picture.

To obtain data on bubble collapse, it is necessary to know the

pressure and temperature quite accurately. The pressure is measured by a circular disc of barium titanate one-half inch in diameter and one-tenth inch thick. The barium titanate disc is a pressure sensitive piezoelectric transducer having a frequency response range (about 20 to 10^5 cycles per sec) more than adequate to provide for good reproduction of the form of the applied pressure. This pressure is recorded photographically from an oscilloscope screen for each bubble collapse. The oscilloscope with recording camera in place is shown in Fig. 41. A single sweep of the oscilloscope trace is initiated by the bubble detector in time to record the pressure rise. Immediately after each pressure record is taken a 1000 cycle tuning fork records one millisecond timing marks on the same photograph. Amplitude calibration of the pressure record is automatic since one flat on the pressure curve corresponds to the static pressure in the container as read by a mercury manometer, and the other flat corresponds to known atmospheric pressure. In order to obtain correspondence between the bubble photographs and the pressure record, it was arranged for a bright spot to appear on the pressure trace at the beginning of the series of pictures and a dark spot to appear at the end. These reference marks were obtained by modulating the oscilloscope beam intensity with the keying signal to the Kerr cell pulser. Records of such traces are shown in Fig. 42. The temperature was recorded by a standard precision mercury thermometer graduated in tenths of a degree centigrade. "O" ring seals were used to permit insertion of the thermometer into the partially evacuated liquid container.

Operation of the equipment was satisfactory as long as no special effort was made to reduce the air content of the distilled water. The study of bubble collapse with small air content was greatly desired,

however, and this fact made operation of the equipment more difficult. The reason for this was simply because the water attained 5^{o} or 6^{o} C of superheat after it had been boiled at reduced pressure for about an hour. The frequency of bubble formation then became very low, and the bubble growth rate became extremely rapid. As a result, the equipment would run for fifteen or twenty minutes and then trip on a bubble already grown much too large. In order to solve this difficulty it was necessary to construct a device which would generate a bubble with small gas content. The first device tested was a thin glass rod coated with a silicone water repellent (Dow Corning Type 200). Bubbles generated in this manner adhered to the rod and grew slowly to a large size before detachment by buoyancy. It was therefore fairly certain that an appreciable amount of air would have time to diffuse into the bubble.[10] This belief was verified by failure of these bubbles to collapse to a small minimum radius. Another type of generator consisted of a 0.005-in. diameter chromel wire etched down to a much smaller diameter over a very short section. This wire was immersed in the water and acted as a heat source when electrical current was passed through it. The applied voltage was kept low (1.5 volt) to minimize electrolysis, but these bubbles also contained excessive gas. It should be mentioned here that an approximate method of estimating gas content was to observe the size of the residual bubble after its radius had reached a steady state. Another bubble generator consisted of a 0.5 cc glass boiling chamber with a resistance wire heater and with a small opening to the surrounding water. As there was nothing but glass in contact with the water, it was expected that there would be little gas present. This generator did not prove to be practical because the initial vapor-water interface was established with too much violence,

and once a cavity existed, trouble was again experienced from air diffusion into the cavity. The only type of bubble generator which proved fairly successful is shown in Fig. 43. Three models are shown, but they differ only in size and shape. This generator consists of two wire electrodes, one of which is sealed into a glass chamber or tube. The opposite end of the tube from the inner wire is open to the water and the other wire is outside of the tube and in contact with the surrounding water in the large container. By repeated raising and lowering of the container pressure all gas is removed from the glass tube. This degassed condition is evidenced by the failure of any interface to form in the tube when the pressure is lowered to less than vapor pressure. When this state is reached, a hydrogen bubble of just sufficient size to grow is generated in the tube at the end of the enclosed wire. Growth is very rapid and the entire tube empties itself at once with the water being replaced by its own vapor. The resultant bubble which emerges from the end of the tube is thus composed of a mixture of hydrogen and water vapor. However, the hydrogen content is extremely small, since it has been subject to a volume dilution in the ratio of the volume of the entire tube to that of the original hydrogen bubble which was just larger than the critical size required for growth.

Observations

Bubbles 3 and 4 plotted in Fig. 44 and shown in Figs. 46 and 47 represent the general trend in the experimental results. The theoretical curves were calculated from spherically symmetric theory in the same manner as were the water tunnel bubbles. In both cases the actual collapse time is longer than the theoretical. It is felt that this discrepancy is real, although greater precision in recording the applied pressure is

desirable. Departure from spherical symmetry is also too large to permit much accuracy in measurement of the bubble. Bubbles 3 and 4 were formed by the glass tube generator described earlier. The size of the residual gas bubble was estimated for each case and a term was included in the equation of boundary motion to represent adiabatic compression of the estimated amount of gas. The pressure resisting collapse due to this gas is approximately proportional to the inverse fourth power of the bubble radius. The adiabatic pressure would be exactly proportional to the inverse fourth power of the radius if the ratio of specific heat at constant pressure to the specific heat at constant volume were 4/3.

For bubbles 3 and 4 this means that presence of the gas has negligible effect on the collapse within the range of observation. The increased collapse time must therefore be due to other factors.

Bubbles 6, 10, and 11 plotted in Fig. 45 and shown in Figs. 48 and 49 are cases where rebound was not observed. Unfortunately, the photography was too poor to justify comparison with theory. It may be noticed, however, that the maximum radial velocity resolved is of the order of 100 ft per sec. This corresponds to a Mach number of 0.02, and hence compressibility effects should be small in the observable range. This does not mean that compressibility effects are negligible at very late stages in the collapse. It only means that the picture rate of 10^5 frames per sec is still too slow for the necessary time resolution. The failure to obtain data at higher rates in this investigation was due only to lack of a mirror and motor capable of rotational speeds greater than 25,000 rpm. It is readily apparent from the photographs that the bubbles are much less stable during collapse than they are during growth. These observations are in general accord with a theoretical study by Plesset.[22] If

spherical symmetry is not preserved, we must solve a much more difficult analytical problem. Few cases in this experimental work are even fair approximations to the spherical shape. For this reason, the original objective of studying the final stages of spherical collapse had to be deferred in favor of studying the available data on the nonspherical case. That such should be the situation was not entirely unexpected, as it was clear from earlier theoretical work[23] that the collapse would be affected by gravity. Modification of the apparatus to permit observation of collapse under free-fall conditions was seriously considered, but such experiments are being deferred to a later date.

In order to discuss the pertinent features of the photographic data it is necessary to write the appropriate equations for the nonspherical case including hydrostatic pressure and upward velocity induced by buoyancy. Departures from the spherical are treated as small perturbations.

The coordinate system is set up with θ measured from the vertical and with a stationary origin which is the centroid of the bubble at time $t = 0$. R is the distance to the bubble boundary, and r is the distance to any point in the liquid. The velocity potential is[9]

$$\varphi\ (r,t) = \sum_{n=0}^{\infty} \frac{\varphi_n(t)\, P_n(\cos\theta)}{r^{n+1}} \qquad (1)$$

where the $\varphi_n(t)$ are functions of time. If the bubble boundary is given in the form

$$f(r,\theta,t) = 0\ ,$$

then the condition that it always contains the same particles is given

by:

$$\frac{df}{dt} = \frac{\partial f}{\partial t} + \bar{q} \cdot \nabla f \tag{2}$$

where $\bar{q}$ is the velocity of the fluid relative to the moving coordinate system. If the form of f is taken to be

$$r - R(\theta, t) = 0 \tag{3}$$

then (2) becomes

$$\frac{dR}{dt} = q_r - q_\theta \frac{1}{R} \frac{\partial R}{\partial \theta} \quad . \tag{4}$$

In Eq. (4) q_r and q_θ are

$$\begin{aligned} q_r &= V_r(r, \theta, t) - V(t) \cos \theta \\ q_\theta &= V_\theta(r, \theta, t) + V(t) \sin \theta \end{aligned} \tag{5}$$

where V(t) is the velocity of the moving origin of coordinates, and V_r and V_θ are the velocities in the r and θ directions, respectively, in the stationary coordinate system.

R may be written in the form

$$R(t) = \sum_{n=0}^{\infty} R_n(t) P_n(\cos \theta) \tag{6}$$

where $R_1 = 0$ because the origin is translating with the bubble.

Substitution of (5) into (4) gives

$$\frac{dR}{dt} = V_r - V \cos \theta - \frac{1}{R} (V_\theta + V \sin \theta) \frac{\partial R}{\partial \theta} \quad . \tag{7}$$

Up to this point there have been no restrictions imposed, but further work becomes very laborious unless the higher order terms in V are neglected. The only purpose here is to show the method of attack. The following development neglects terms of the order of V^4, and is taken from "Underwater Explosions" by Cole[24]. Eq. (7) becomes

$$\frac{dR}{dt} = \left(-\frac{\partial\varphi}{\partial r}\right)_R - V\cos\theta = \frac{\varphi_o}{R^2} + \frac{2\varphi_1}{R^3} P_1 + \frac{3\varphi_2}{R^4} P_2 + 0(V^4) \qquad (8)$$

$\frac{dR}{dt}$ may also be obtained by differentiating (6). When this is done, the coefficients of like P's must be equal, as the expression must be true for any θ. Substitution for R and $\frac{dR}{dt}$ then gives the relations

$$\varphi_o = R_o^2 \frac{dR_o}{dt} \; ; \quad \varphi_1 \left(1 - \frac{6}{5}\frac{R_2}{R_o}\right) = \frac{1}{2} R_o^3 V \; ; \qquad (9)$$

$$\frac{dR_2}{dt} + \frac{2\varphi_o}{R_o^3} R_2 = \frac{3\varphi_2}{R_o^4} \; ; \quad \frac{dR_3}{dt} + \frac{2\varphi_o}{R_o^3} R_3 = \frac{4\varphi_3}{R_o^5} - \frac{18}{5}\frac{\varphi_1}{R_o^4} R_2 \; .$$

Bernoulli's equation may be written

$$\left(\frac{\partial\varphi}{\partial t}\right)_R - \frac{1}{2}(\nabla\varphi)_R^2 = \frac{P_v - P_o}{\rho} + gR\cos\theta \qquad (10)$$

where P_o is the hydrostatic pressure at the bubble center. Substitution for R and φ then gives a series of terms in the Legendre polynomials. Multiplying the Bernoulli equation by P_o, P_1, P_2, and P_3 in turn and making use of the orthogonality relation leads to the

following set of equations:

$$R_o \frac{d^2R_o}{dt^2} + \frac{3}{2}\left(\frac{dR_o}{dt}\right)^2 - \frac{P_v - P_o}{\rho} + 0(V^4) - \frac{V^2}{4} = 0 \tag{11}$$

$$\frac{1}{2}\frac{d}{dt}(R_o^3 V) - \frac{6}{5} g \int \frac{\varphi_2}{R_o^2}\, dt - g R_o^3 + 0(V^3) = 0 \tag{12}$$

$$\frac{1}{R_o^3}\frac{d\varphi_2}{dt} - \frac{3\varphi_2}{R_o^4}\frac{dR_o}{dt} + \frac{3}{4}V^2 - \frac{1}{R_o^2}\frac{d^2R_o}{dt^2}\int \frac{3\varphi_2}{R_o^2}\, dt + 0(V^3) = 0 \tag{13}$$

$$\frac{1}{R_o^4}\frac{d\varphi_3}{dt} - \frac{4\varphi_3}{R_o^5}\frac{dR_o}{dt} \quad \frac{1}{R_o^2}\frac{d^2R_o}{dt^2}\int \frac{4\varphi_3}{R_o^3}\, dt + 0(V^3) = 0 \ . \tag{14}$$

Note that for zero translational velocity, (11) reduces to the equation used in the first part of this work. Furthermore, if φ_2, which is of order V^2, is neglected, (12) may be integrated to give Herring's formula for the bubble rise:

$$V = \frac{2g}{R_o^3}\int R_o^3\, dt \ . \tag{15}$$

This formula may also be obtained simply by equating the buoyant force acting on the bubble to the rate of change of upward momentum of the entrained liquid. By itself, it is obviously in error for small R_o since V tends to infinity. The bubble drag as well as the term in φ_2 must be considered. However, Eq. (15)

qualitatively explains the rapid upward jump of the bubble very near the minimum radius. This effect is larger if the bubble has acquired large upward momentum before collapse begins. This conclusion is in agreement with experimental observation. Bubbles 3 and 4 show a negligible effect of this type, and they were collapsed close to the bubble generator before much upward momentum was attained. In contrast, bubble 24 had moved upward through the fluid for a considerable distance. It should be noted that the center portion of the bubble tends to speed up more rapidly. This induces vorticity and gives rise to vortex rings seen in Figs. 51, 52, and 53. The entire theory outlined here breaks down in these cases.

It was suspected that there might be effects present due to the proximity of the container walls. A new container providing at least two inches distance between the bubble and any wall or surface was therefore constructed. This was about twice the linear dimensions of the previous container and provided a wall distance to radius ratio of about twenty. Bubble 50 shown in Fig. 54 was photographed in this larger container. It possesses similar characteristics to bubbles 21 and 29 which were photographed in the vessel with wall and surface clearance of only about ten radii. A check on the pressure in the liquid at the point of bubble formation revealed no measurable pressure waves reflected from the liquid boundaries. This measurement was made by a 0.1 cm barium titanate pressure transducer. Because of this finding, it seemed correct to assume that the bubble asymmetry was due to vertical rise velocity and hydrostatic pressure gradient.

The method of approach to this problem was outlined in the preceding Eqs. (1) to (15). The equations themselves are of little use here because the neglected higher order terms are important. It was thought sufficient to indicate the method at the present time.

In order to determine how many Legendre polynomials are required, an analysis of bubble 21 was made for each frame. This is shown in Fig. 56. The variation with time of each component is apparent and is an indication of the stability of the bubble collapse. The origin was chosen to translate with the bubble centroid. Hence A_1 should remain zero. The value of A_1 is plotted to indicate the accuracy of the choice of origin used in making the measurements. As a further check, frame 8 was drawn from the numerical values obtained for the first five and first six terms. This drawing is shown in Fig. 55. It is apparent that the first five terms give a good representation at this stage of collapse.

VI. CONCLUSIONS

Among the conclusions which may be drawn from the experimental observations, both in the High Speed Water Tunnel and in the small sample of stationary water, the following may be listed here:

1. Asymmetry in the Collapsing Bubble Shape. It was a consistent finding in these experiments that the collapsing bubbles showed increasing departures from the spherical shape with decreasing radius. A graphic indication of this effect may be observed in Fig. 56. A quantitative demonstration of the increase in asymmetry is brought out if one considers A_2/A_0, A_3/A_0, etc., where A_n is the coefficient of the n'th Legendre polynomial P_n and A_0 is the mean radius as a function of time. There are two possible causes of this asymmetry: a basic instability of a collapsing gas cavity in a liquid, and the collapse in a pressure gradient. Of these the latter is presumably of greater importance in the present experiments. The basis for this supposition is that the asymmetries observed were confined primarily to small values of n in the Legendre polynomial expansion. The inherent instability of the collapse presumably involves large values of n and smaller radii than were observed here.

2. Increased Collapse Time of the Observed Bubbles. It was found that the time of collapse was appreciably longer than would be expected from the extended Rayleigh theory. This increased collapse time cannot be ascribed to a permanent gas content in the bubble since the mass of permanent gas has been observed to be too small to give the observed discrepancy. Further, the increased collapse time was also found for bubbles which contained practically no permanent gas. This

observation is of theoretical interest. It cannot be ascribed to compressibility effects since the observed collapse velocity range did not reach high enough velocities. The theoretical explanation lies in the asymmetry of the collapse shapes. As Rattray[11] has shown theoretically, departure from the spherical shape in a collapsing bubble produces a significant lengthening of the collapse time.

3. Large Coupling between Radial and Translational Bubble Motion. The equation of motion for a collapsing bubble in a liquid is nonlinear. Consequently, there are to be expected coupling effects between the radial collapse motion and the direction of action of any pressure gradient in the liquid field in the neighborhood of the bubble. This coupling effect has been observed in a very striking manner both in the High Speed Water Tunnel and in the static water sample. The general effect of the coupling is to produce an increase in the translational motion in the direction of decreasing pressure.

4. Rebounding and Nonrebounding Bubbles. Two distinct classes of bubbles were observed both in the High Speed Water Tunnel and in the static water sample. One type of bubble rebounded after collapse and eventually could be seen to be a more or less stationary gas bubble. The second type of bubble did not rebound after the first collapse. It is held that the latter type of bubble contained negligible amounts of permanent gas. This nonrebounding type of bubble was observed much less frequently in the High Speed Water Tunnel than in the static water sample. It appears reasonable to expect that the nonrebounding vapor bubble may be a more important source of cavitation damage and noise than the bubbles containing permanent gas with their cushioned collapse.

5. Bubble Collapse Less Stable than Bubble Growth. The trend of the present observations on bubble behavior indicates that the bubble growth is more stable than bubble collapse. Stability is used here to signify that the bubble retains a spherical shape. There has been increased interest recently in the stability of a liquid-gas interface in accelerated motion. G. I. Taylor[25] has considered the stability of a plane interface, and extensions of this analysis to spherical interfaces have been made by M. S. Plesset.

REFERENCES

(1) Thoma, D., Die Kavitation bei Wasser Turbinen. Hydraulische Probleme V.D.I., Verlag (1926).

(2) Lord Rayleigh, The Pressure Developed in a Liquid During the Collapse of a Spherical Cavity. Philosophical Magazine (1917), Vol. 34, p. 94.

(3) Besant, W., Hydrostatics and Hydrodynamics. Cambridge (1859).

(4) Ackeret, J., Experimental and Theoretical Investigations on Cavitation in Water. Technische Mechanik und Thermodynamik. Forschung (1930) Vol. 1 No. 1.

(5) Gilmore, F. R., The Growth or Collapse of a Spherical Bubble in a Viscous Compressible Liquid. California Institute of Technology Hydrodynamics Laboratory Report No. 26-4 (1952)

(6) Knapp, R. T., and Hollander, A., Laboratory Investigations of the Mechanism of Cavitation. Transactions American Society of Mechanical Engineers (1948), Vol. 70, p.419.

(7) Plesset, M. S., Dynamics of Cavitation Bubbles. Journal of Applied Mechanics (1949), Vol. 16, p. 277.

(8) Plesset, M. S., and Zwick, S. A., A Non-Steady Heat Diffusion Problem with Spherical Symmetry. California Institute of Technology Hydrodynamics Laboratory Report No. 26-3 (1951)

(9) Lamb, H., Hydrodynamics. Dover (1945), pp. 37-43.

(10) Epstein, P. S., and Plesset, M. S. On the Stability of Gas Bubbles in Liquid-Gas Solutions. Journal of Chemical Physics (1950), Vol. 18, pp. 1505-1509.

(11) Rattray, M., Perturbation Effects in Cavitation Bubble Dynamics. California Institute of Technology Ph.D. Thesis (1951).

(12) Bowen, I. S., Unpublished work which will be reported by the U. S. Naval Ordnance Test Station, Inyokern, California.

(13) Miller, C. D., and Shaftan, K. High-Speed Photography in Design. Product Engineering. McGraw-Hill (September 1952)

(14) White, H. J., The Technique of Kerr Cells. Review of Scientific Instruments (1935) Vol. 6, pp. 22-26.

(15) Cady, W. M., and Zarem, A. M., Brief Pulses Using Kerr Cells. Nature (1948), Vol. 162, No. 4118, pp. 528-529.

(16) Zarem, A. M., and Marshall, F. R., A Multiple Kerr Cell Camera. Review of Scientific Instruments (1950) Vol. 21, pp. 514-519.

(17) Schmidt, Briggs, and Looschen, Use of High-Pressure Mercury Arc Lamps for Pulsed Light Applications. American Institute of Electrical Engineers Miscellaneous Paper 50-183 (May 1950)

(18) Guillemin, E. A., Communication Networks. Wiley (1935) Vol. 2, pp. 299-375.

(19) Mack, J. E., Optical Methods and Instruments. Miscellaneous Physical and Chemical Techniques of the Los Alamos Project. McGraw-Hill (1952) Vol. 3, pp. 283-317.

(20) Bowersox, R. B., Construction of a High-Speed Motion Picture Camera. California Institute of Technology Jet Propulsion Laboratory Memorandum No. 20-64 (1951).

(21) Glasoe, G. N., and Lebacqz, J. V., Pulse Generators. M.I.T. Radiation Laboratory Series. McGraw-Hill (1948) Vol. 5

(22) Plesset, M. S., Unpublished work to be released soon by California Institute of Technology Hydrodynamics Laboratory.

(23) Herring, C., Theory of Pulsations of the Gas Bubble Produced by an Underwater Explosion. National Defense Research Council Report C4-sr-20-010, (October 1941).

(24) Cole, R. H., Underwater Explosions. Princeton (1948), pp. 309-310.

(25) Taylor, Sir Geoffrey, The Instability of Liquid Surfaces when Accelerated in a Direction Perpendicular to their Planes. I. Proc. Roc. Soc. (1950) Vol. 201, No. 1065, pp. 192-196.

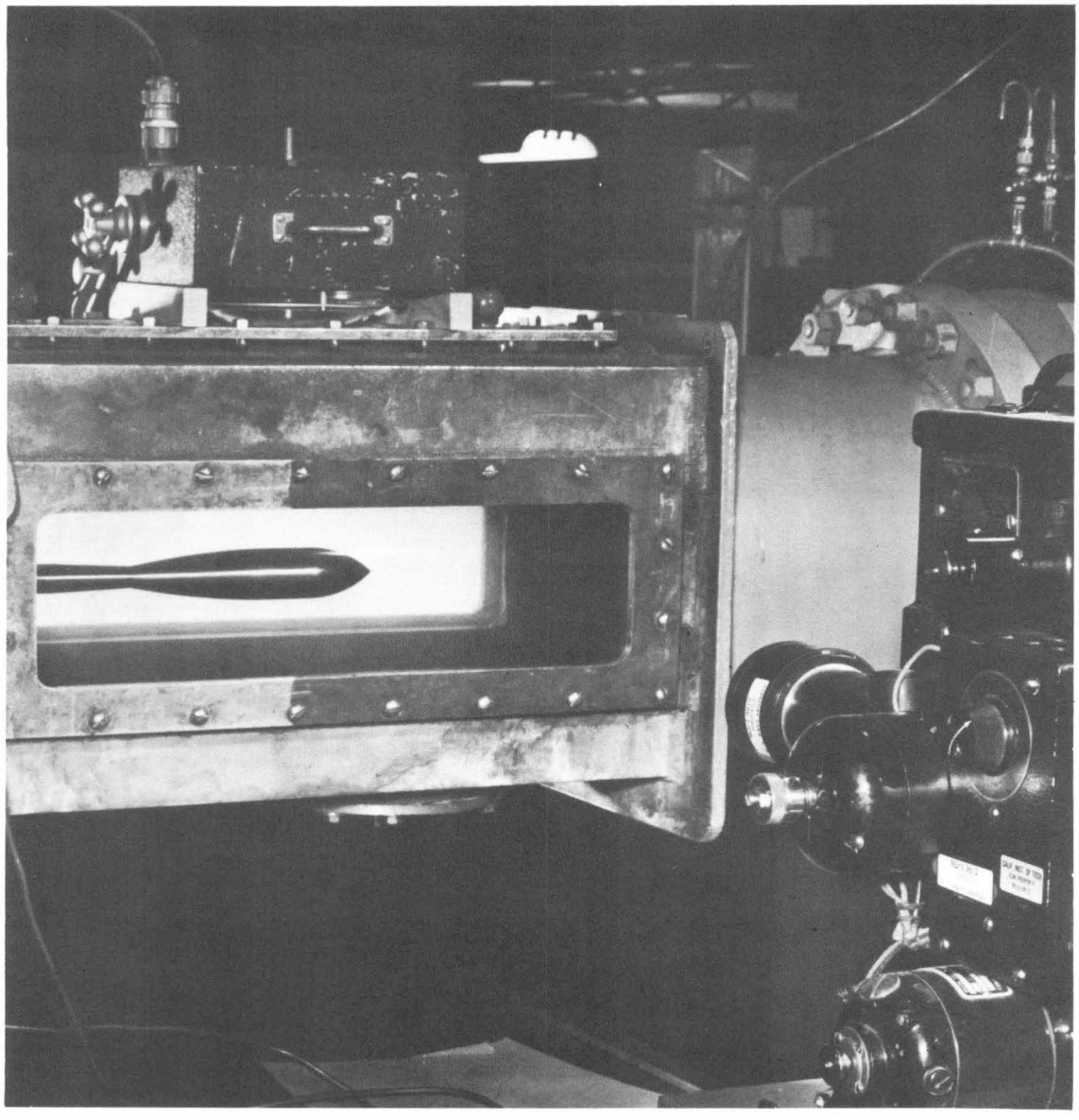

Fig. 1 - Apparatus for taking cavitation bubble photographs in the High Speed Water Tunnel of the Hydrodynamics Laboratory. The sting supported 1.5-caliber ogive model is shown in place. A top lighting arrangement is shown, and the General Radio camera may be seen in the foreground.

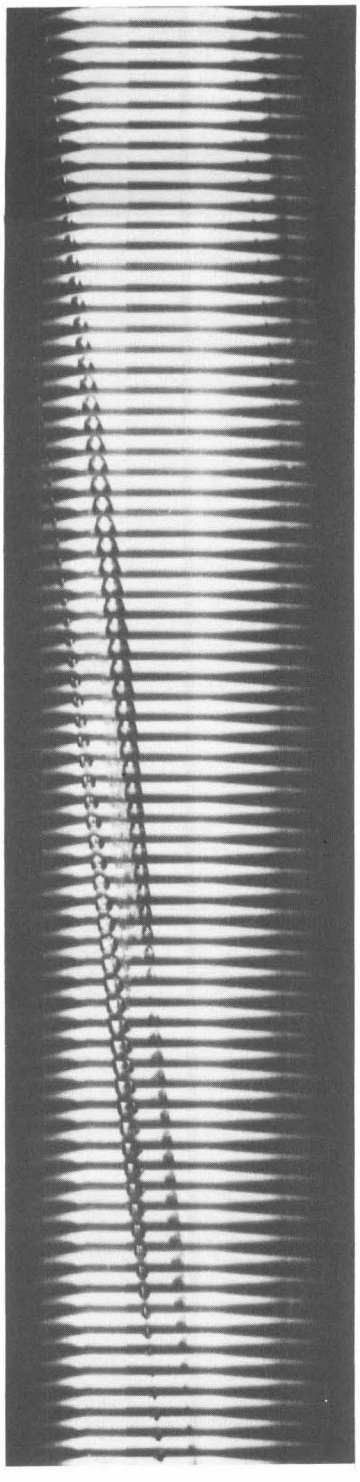

Fig. 2

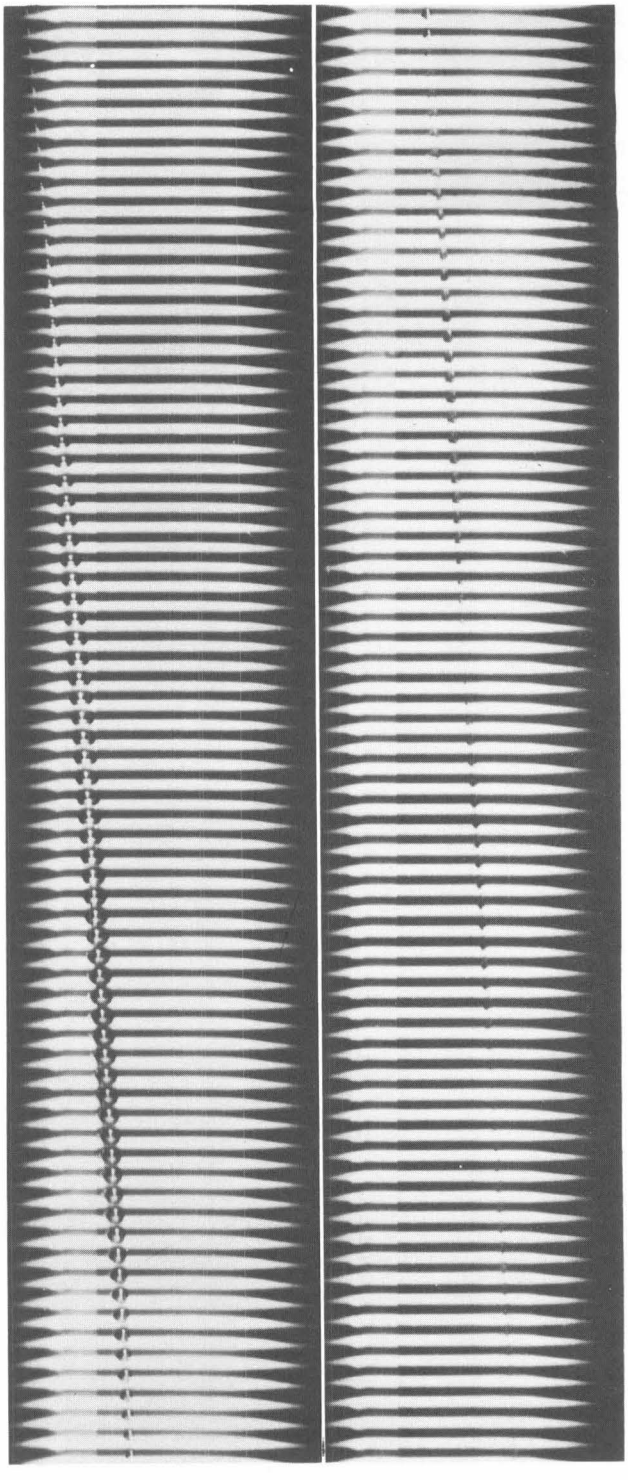

Fig. 3

Cavitation on the 1.5-caliber ogive. These are examples of front lighting photography taken at the rate of 19,000 frames per second.

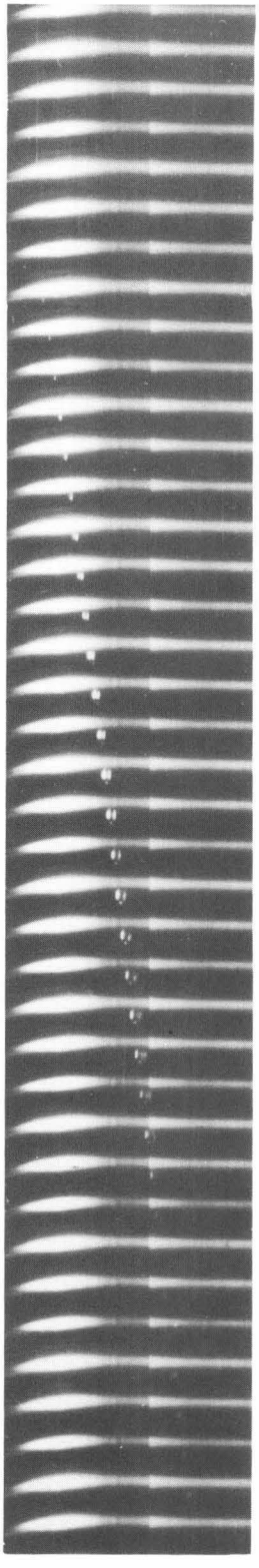

Fig. 4 - Two top lights

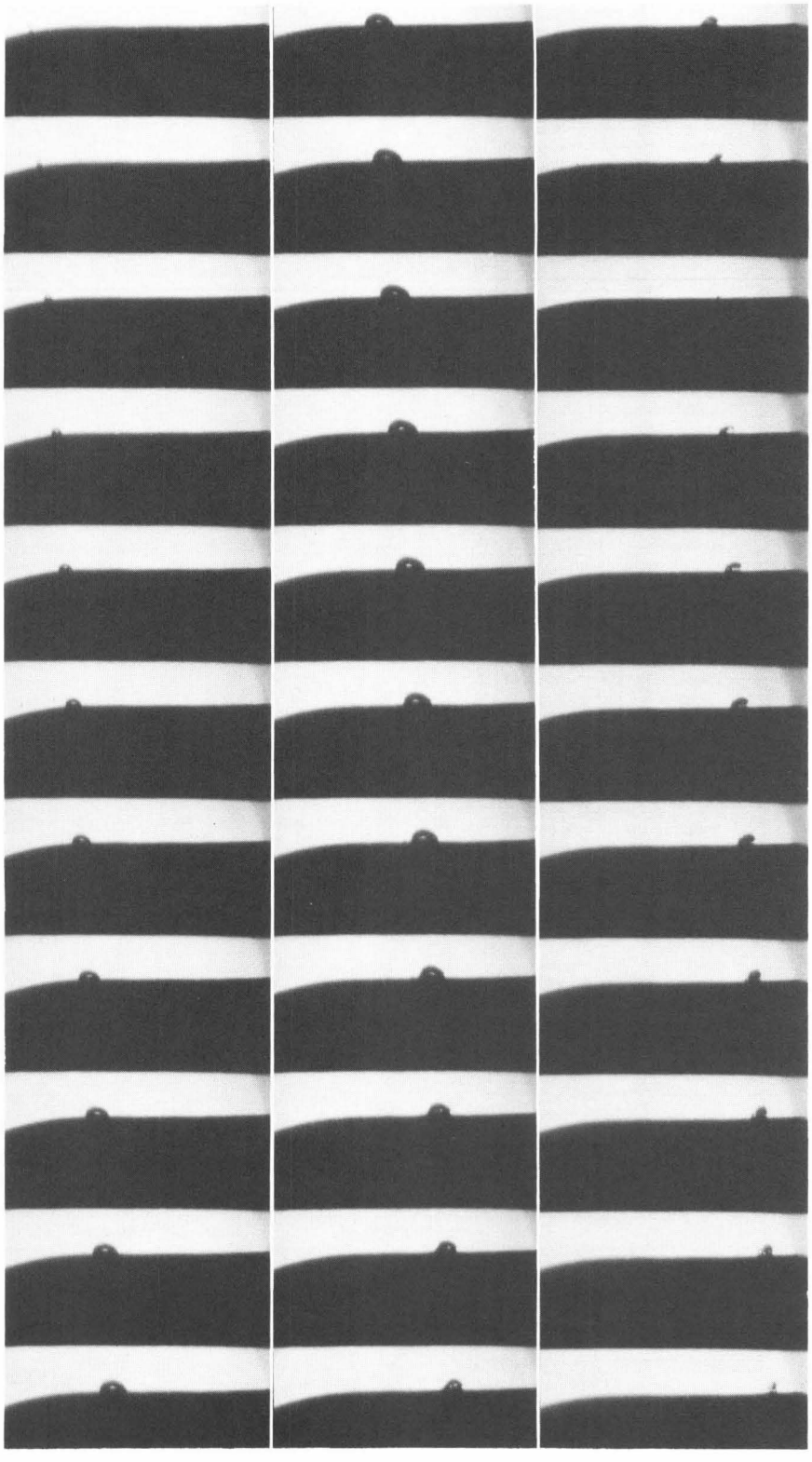

Fig. 5 - Back lighting

Cavitation on the 1.5-caliber ogive.

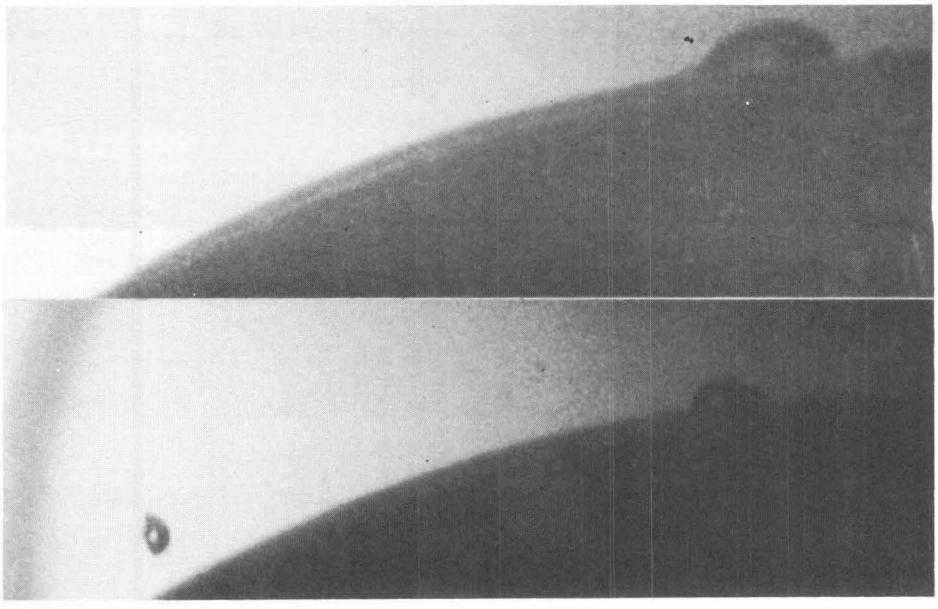

Fig. 6 - Magnified view of 1.5-caliber ogive model surface showing hemispherical surface bubbles and one off surface bubble.

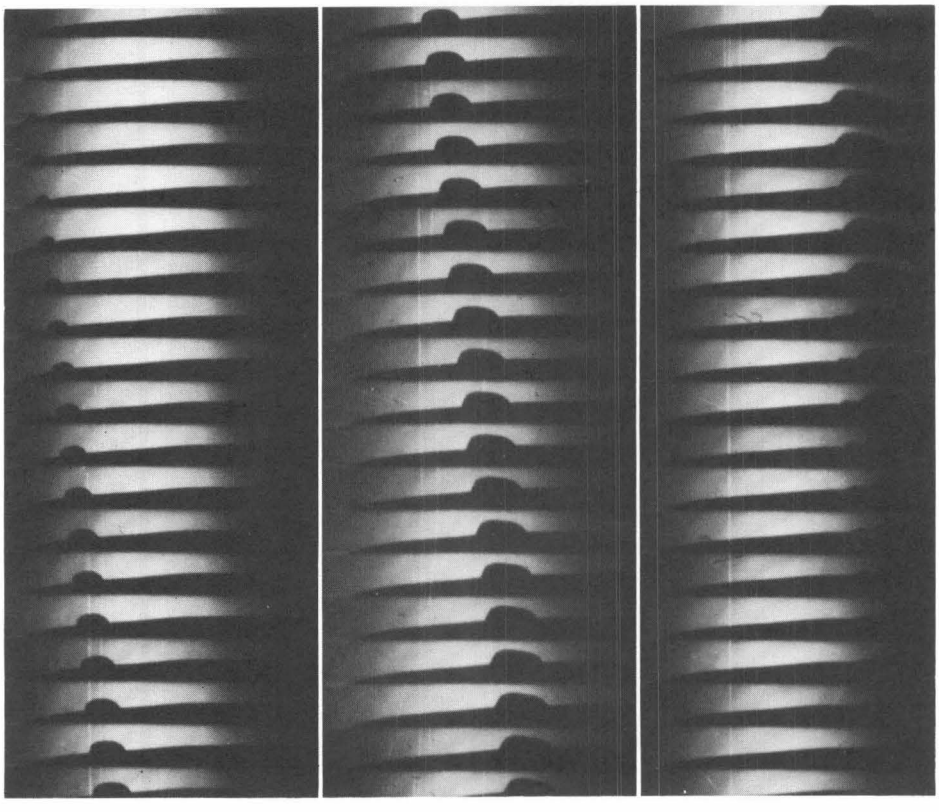

Fig. 7 - Silhouette view of large noncollapsing bubble on half body surface.

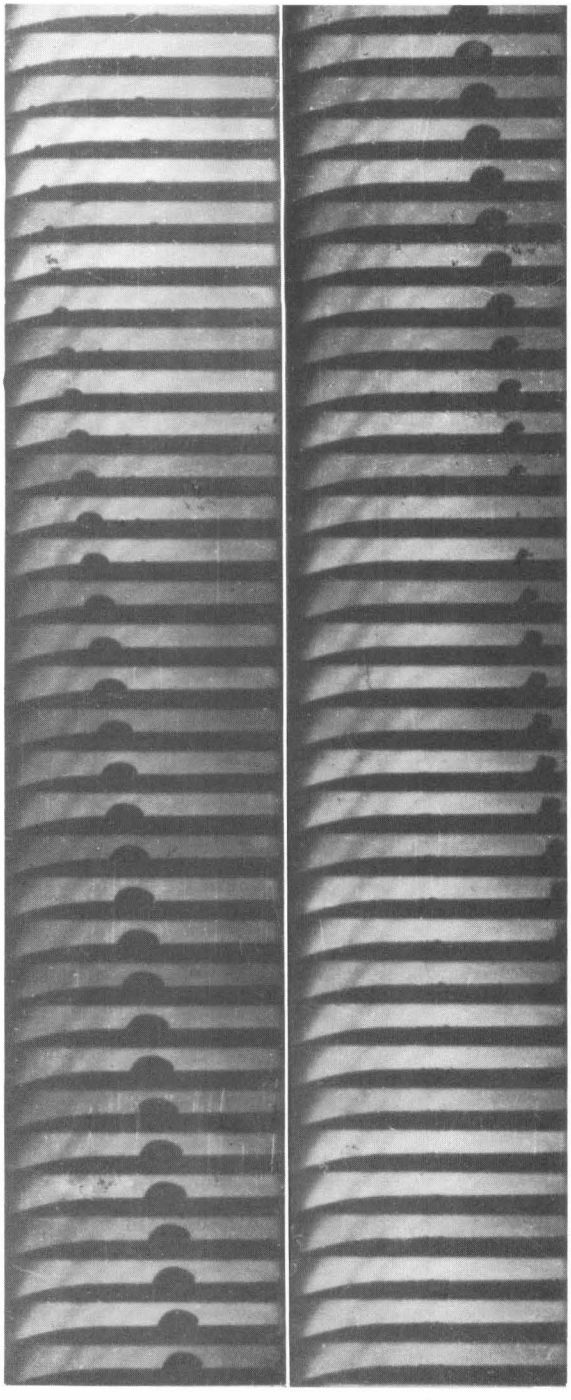

Fig. 8 - Bubble 24
K = 0.271
V = 39.4 ft/sec

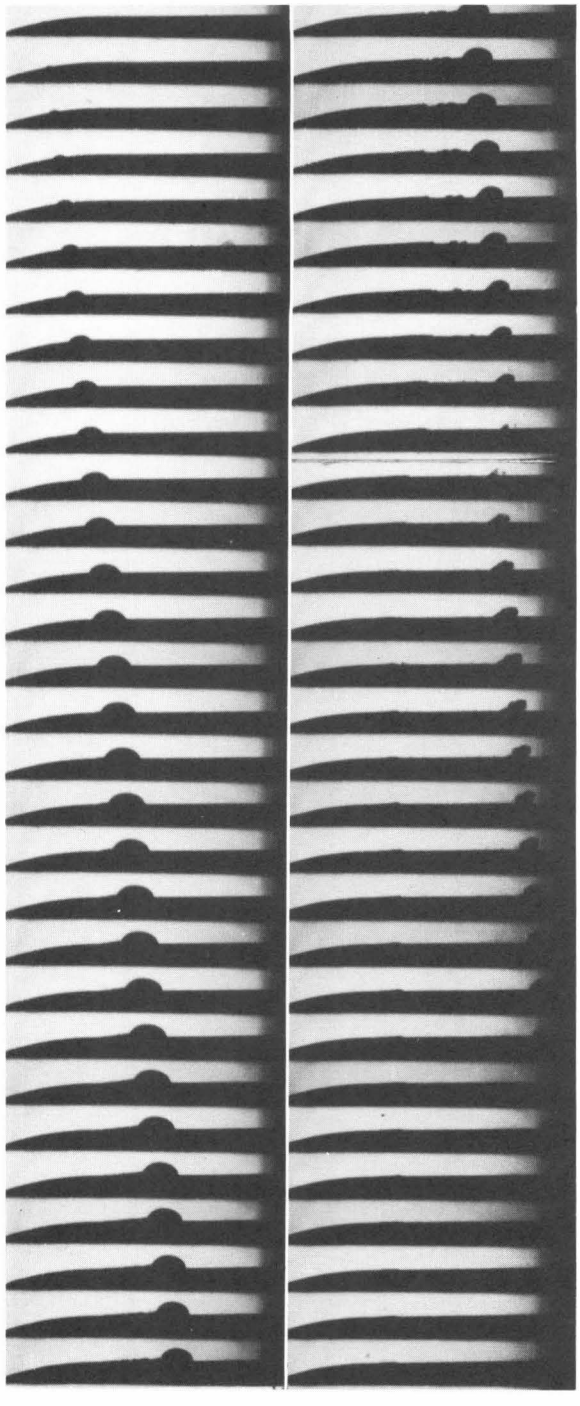

Fig. 9 - Bubble 26
K = 0.279
V = 39.6 ft/sec

Cavitation on 1.5-caliber ogive.
Picture rate: 10,000 frames per second.

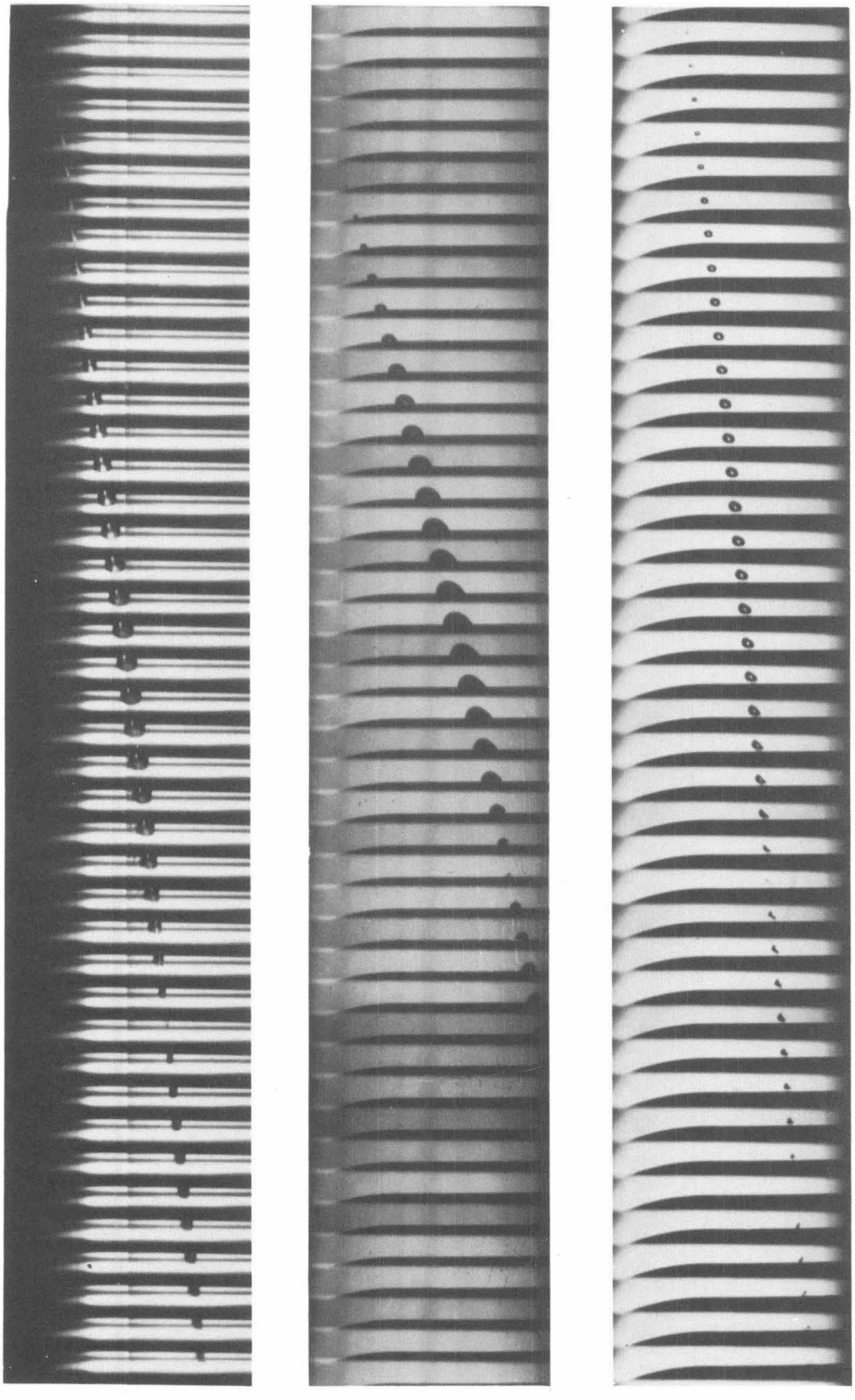

Fig. 10 - Bubble 10
K = 0.295
V = 39.7 ft/sec

Fig. 11 - Bubble 36
K = 0.239
V = 85.34 ft/sec

Fig. 12 - Bubble 27
K = 0.266
V = 39.4 ft/sec

Cavitation on 1.5-caliber ogive.
Picture rate: 10,000 frames per second.

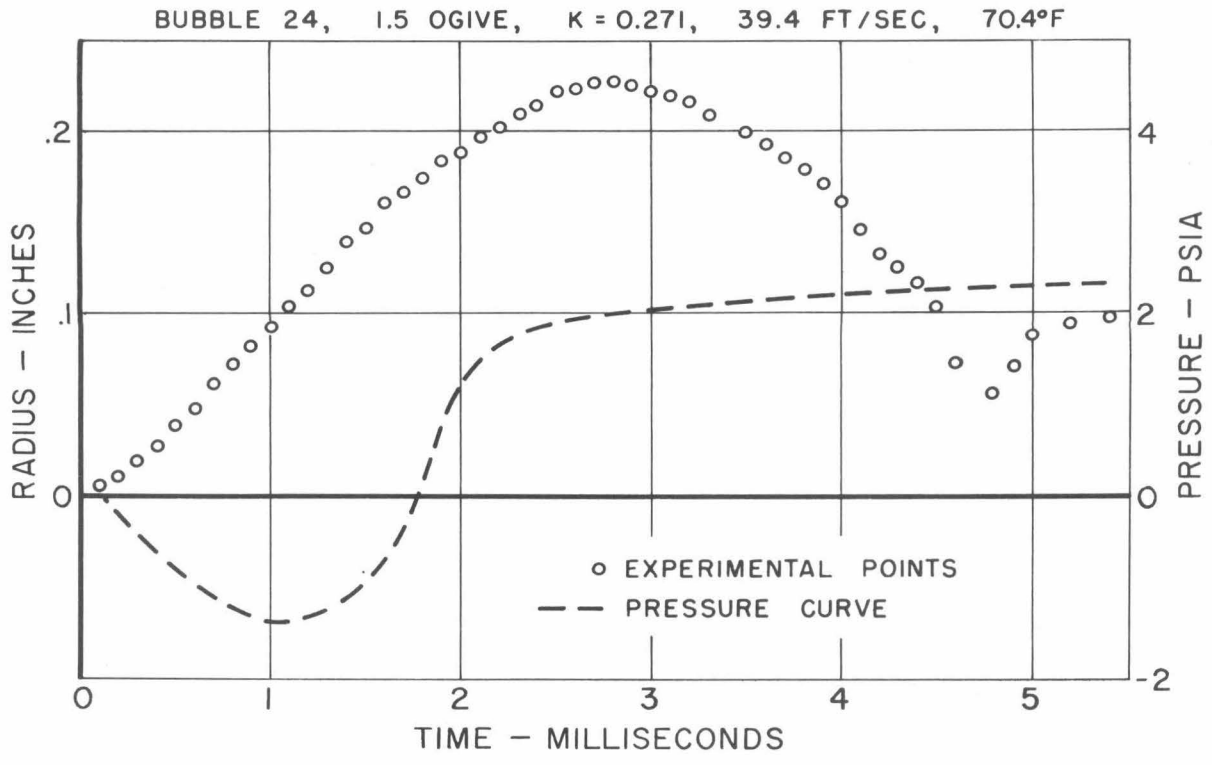

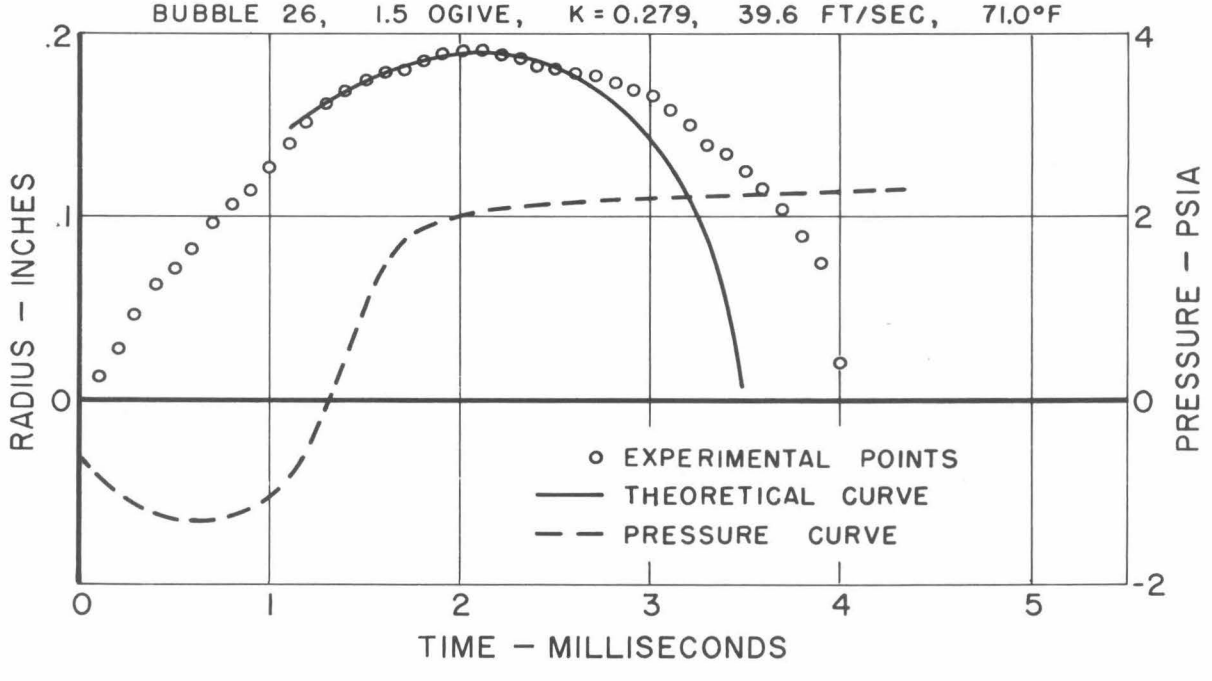

Fig. 13 - Cavitation bubbles on 1.5-caliber ogive model.

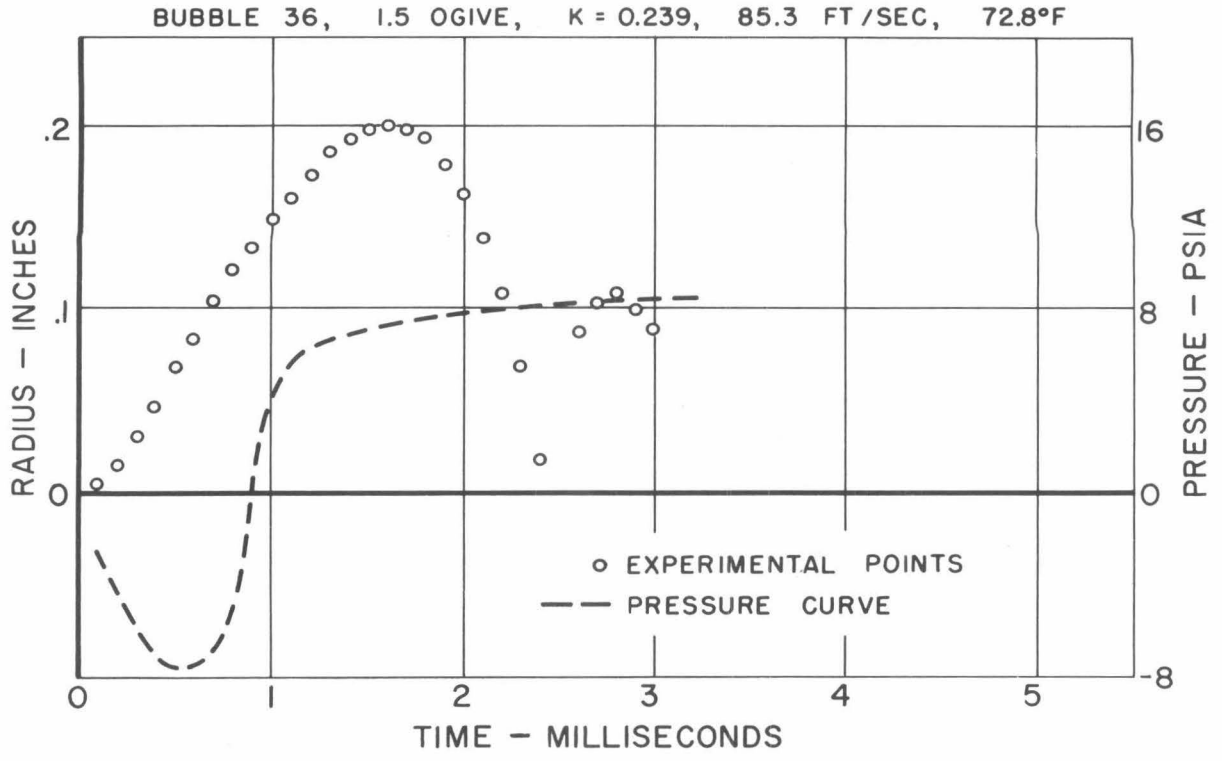

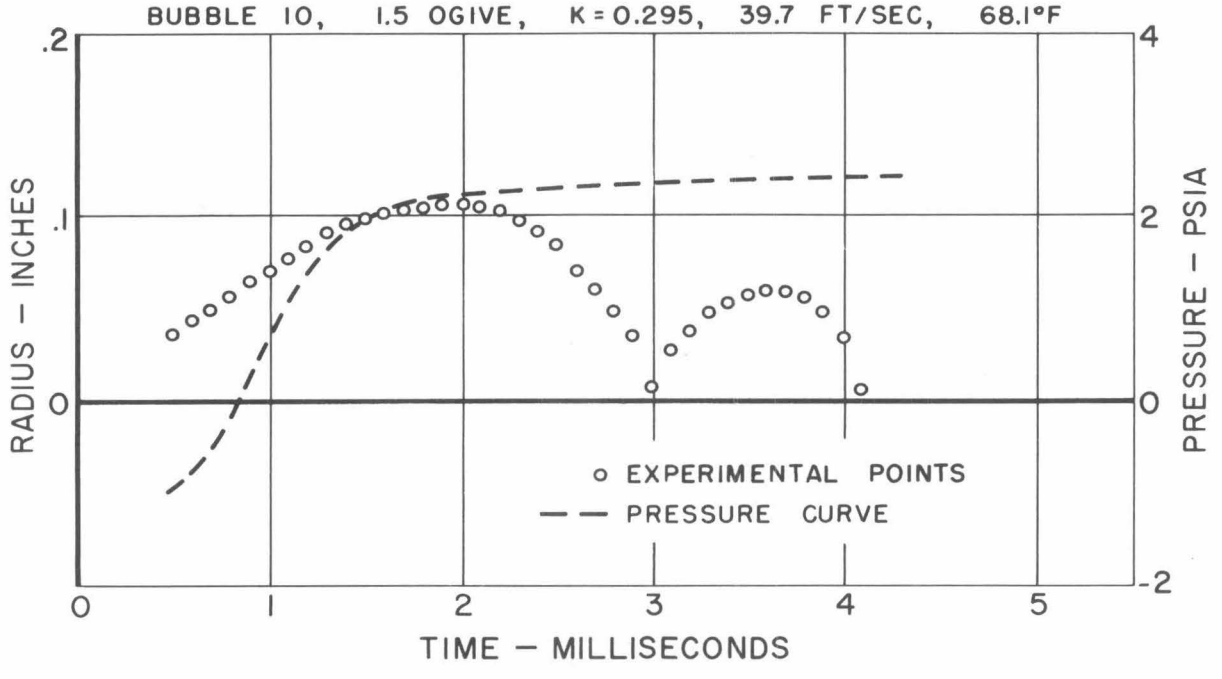

Fig. 14 - Cavitation bubbles on 1.5-caliber ogive model.

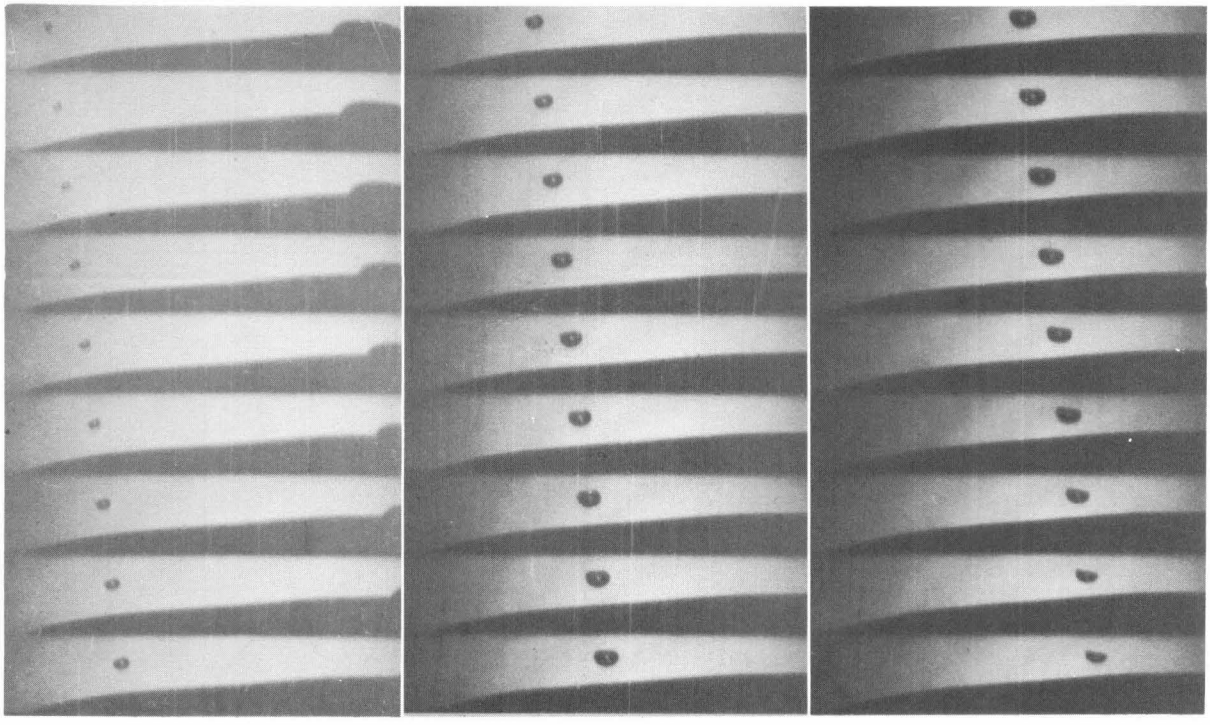

Fig. 15 - Collapsing bubble off surface of half body model. Note movement of flat surface on bubble to remain perpendicular to pressure gradient.

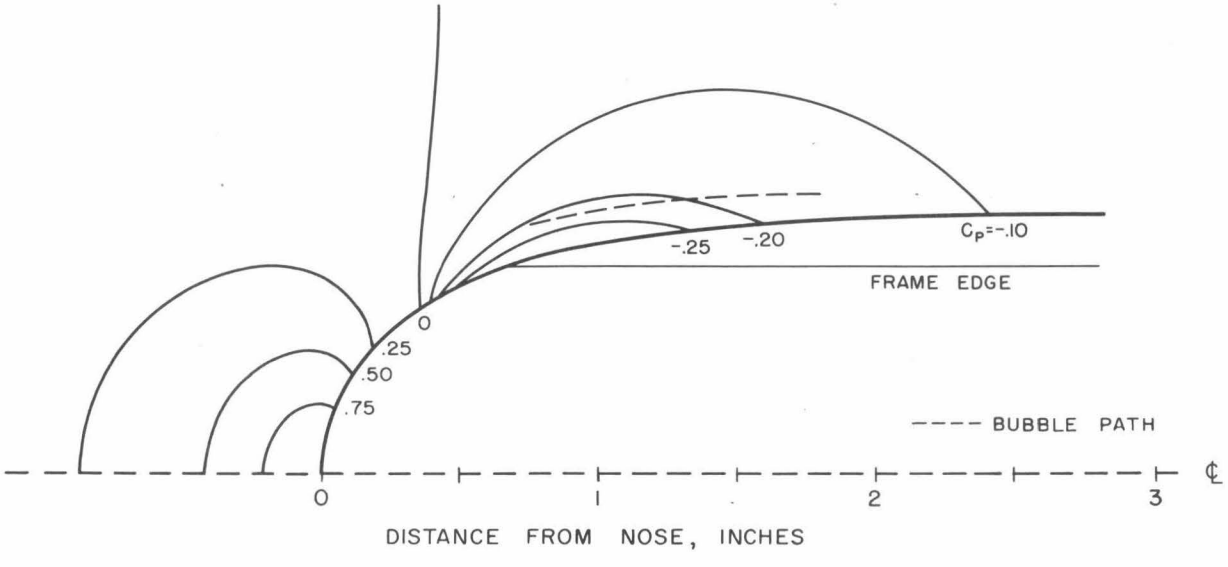

Fig. 16 - Pressure distribution off surface of half-body model.

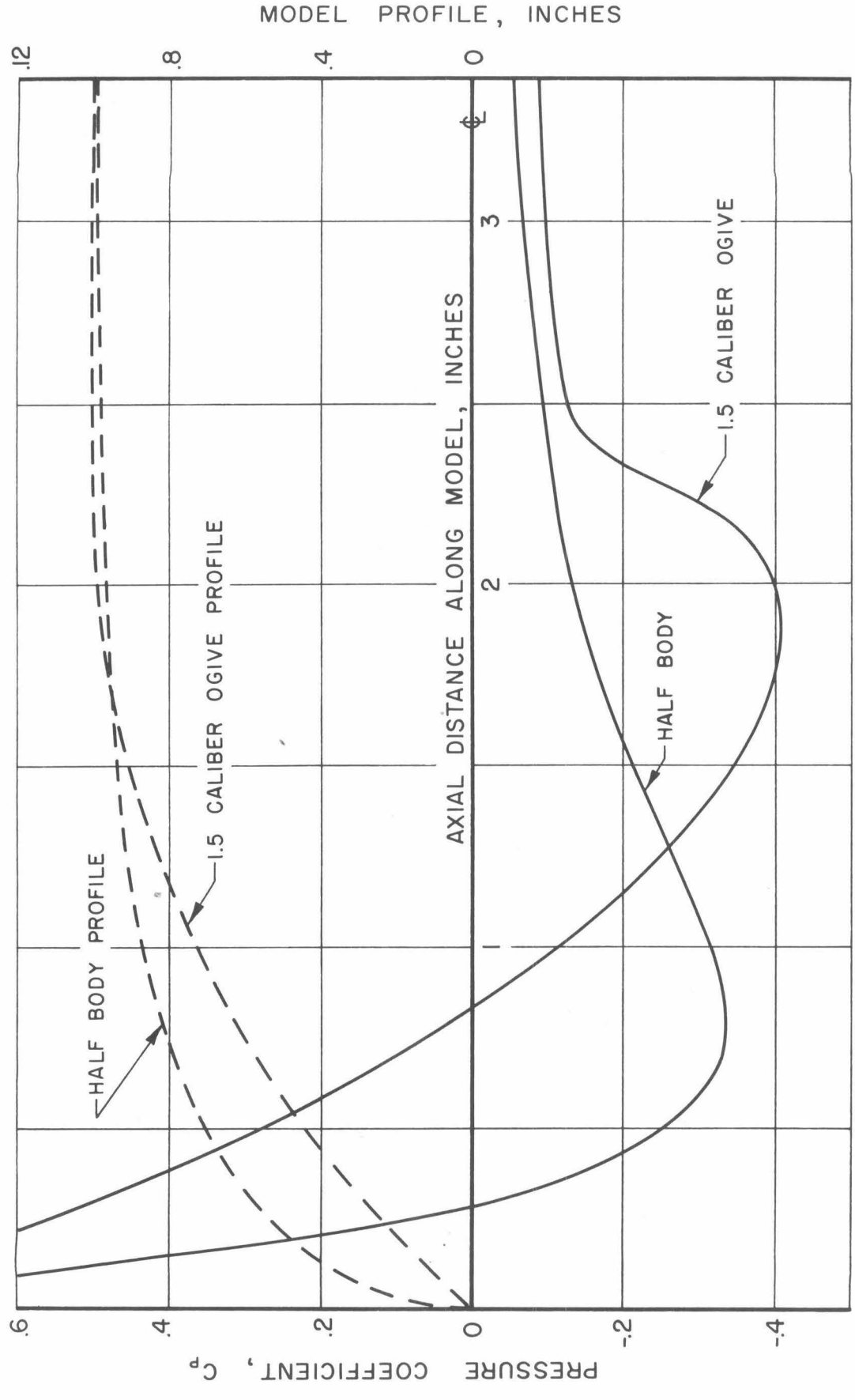

Fig. 17 - Pressure distribution on half body and 1.5-caliber ogive models.

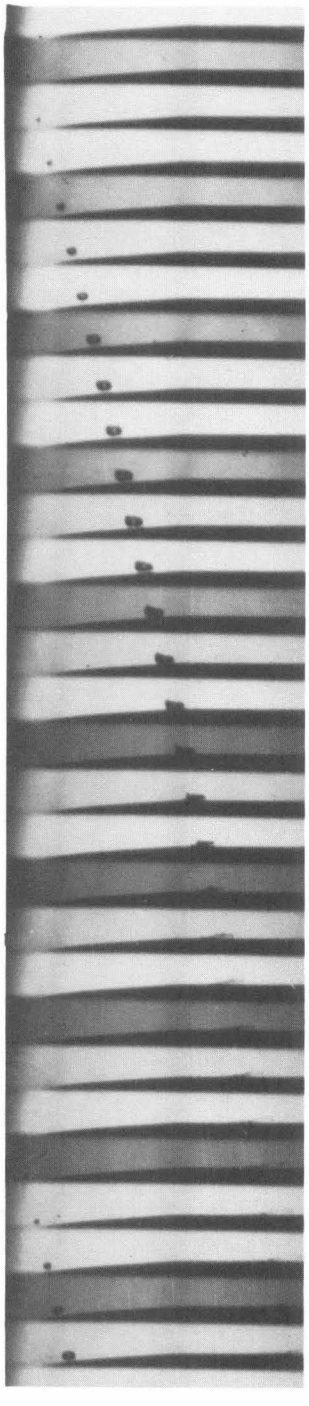

Fig. 18 - Bubble collapsing flat slightly off surface of half body model.

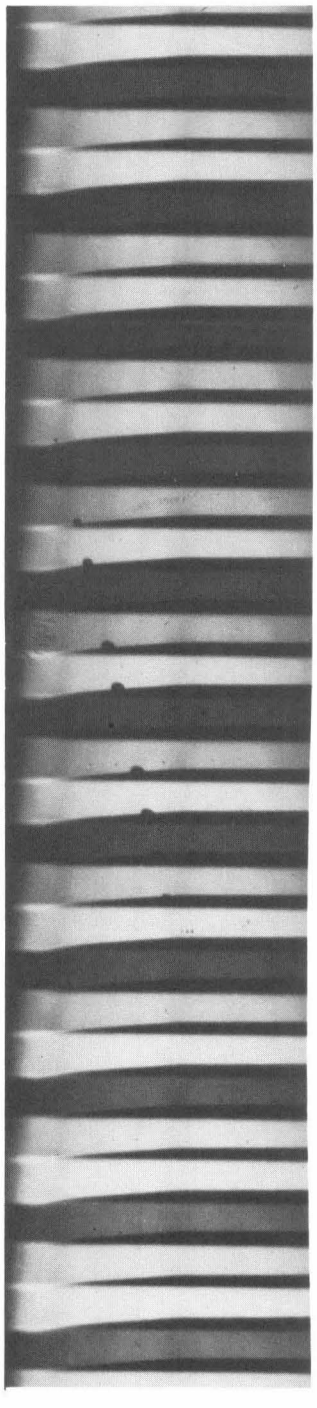

Fig. 19 - Collapse without rebound on surface of half body.

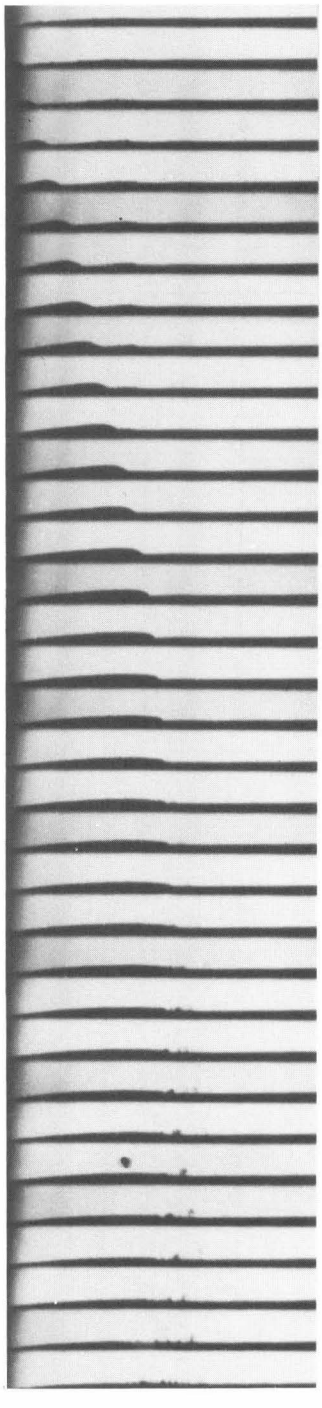

Fig. 20 - Incipient transition to the cavity flow stage.

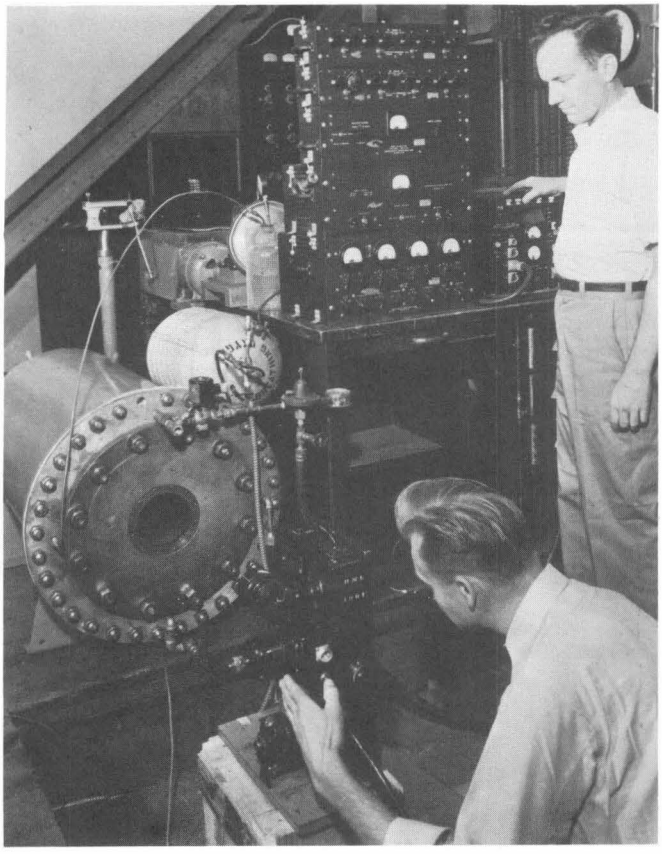

Fig. 21 - Apparatus for collapsing glass spheres in a pressurized tank. The same tank was also used for spark generated bubble study.

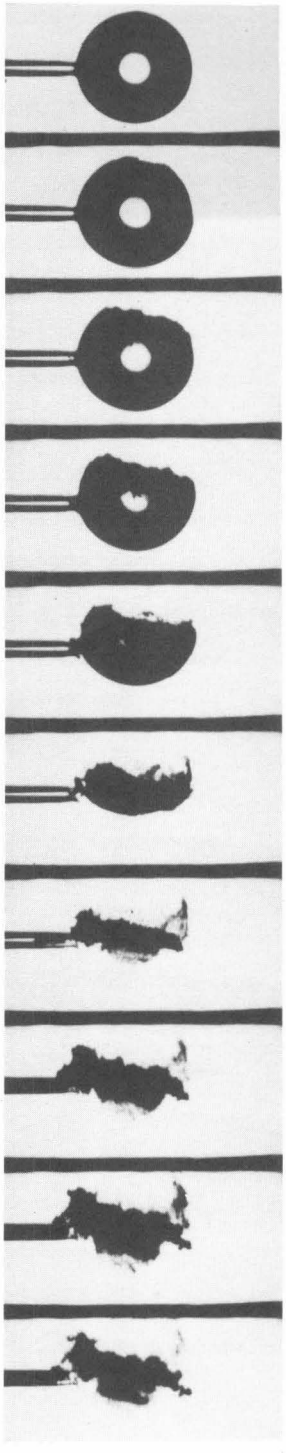

Fig. 22 - A movie record at 1,000 frames per second.

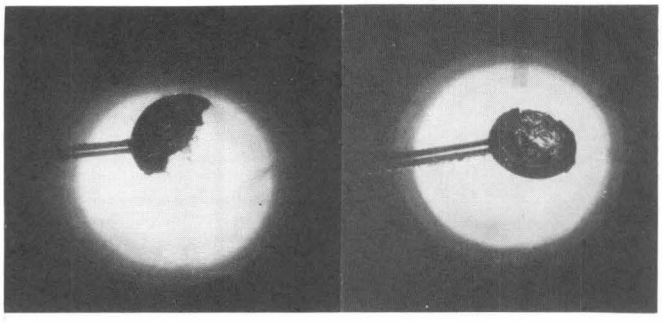

Fig. 23 - Single exposure pictures of glass spheres in process of collapsing.

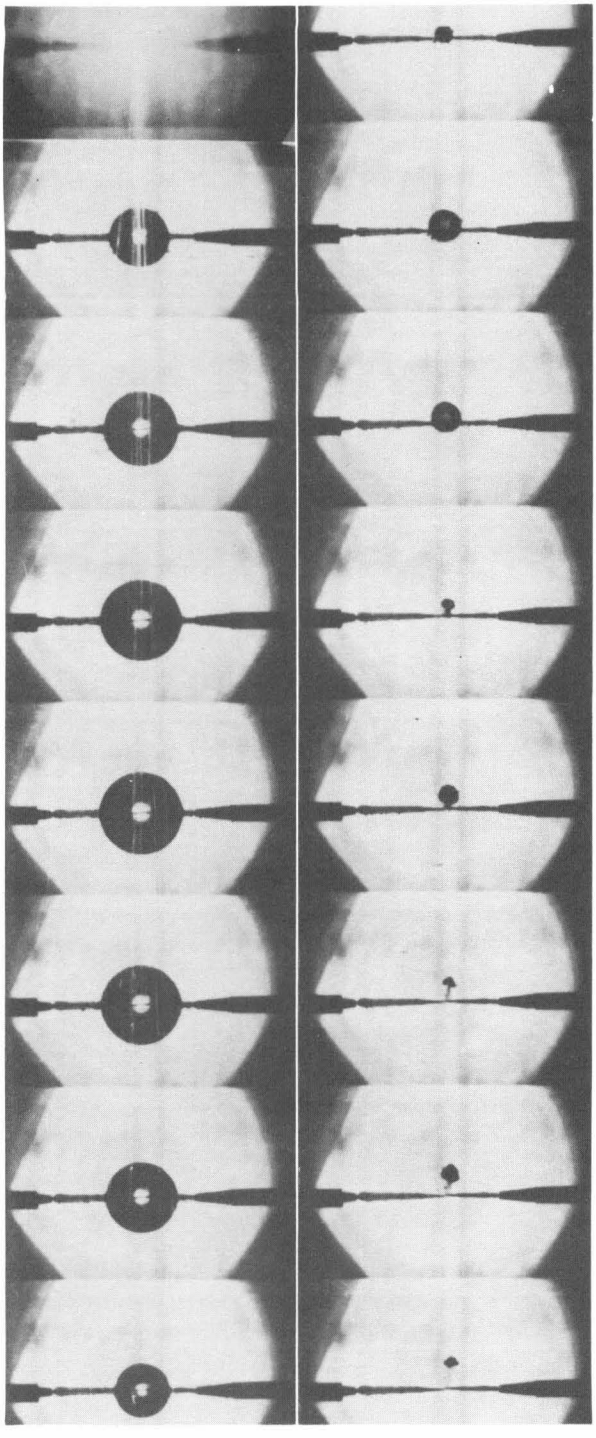

Fig. 24 - Collapsing spark bubble.
P - P_v = 6.01 psia
Max. radius 0.71 in.
Collapse time 0.0027 sec.

Figures 24, 25 and 26 show a collapsing spark bubble with rebounds. Electrical discharge energy is kept constant at 45.6 joules in all runs, and the external pressure is varied. Picture rates are 1500 frames per second, and pictures are 0.31 times actual size in all cases.

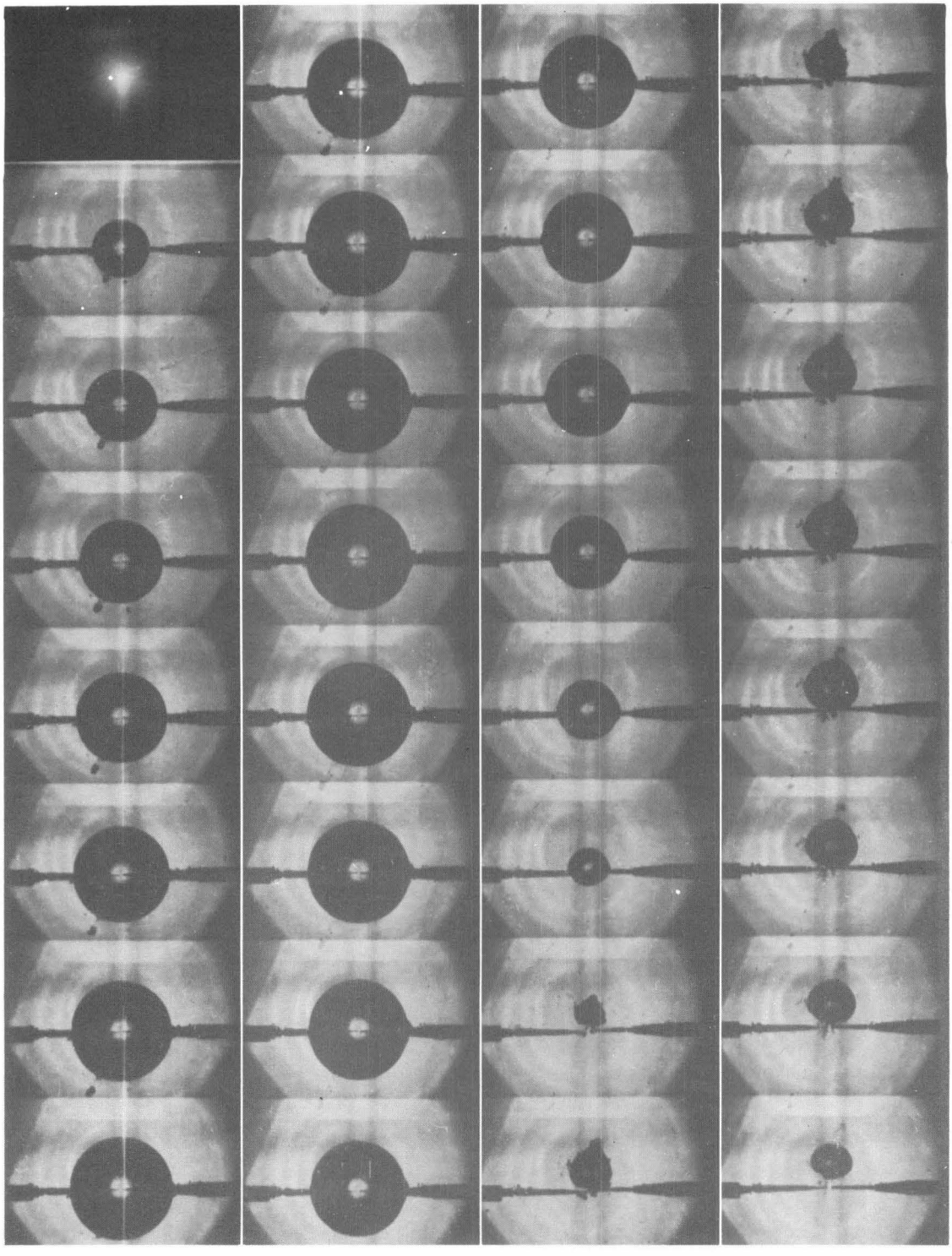

Fig. 25 - Collapsing spark bubble.
$P - P_v = 2.22$ psia; Max. radius 1.09 in.; Collapse time 0.007 sec.

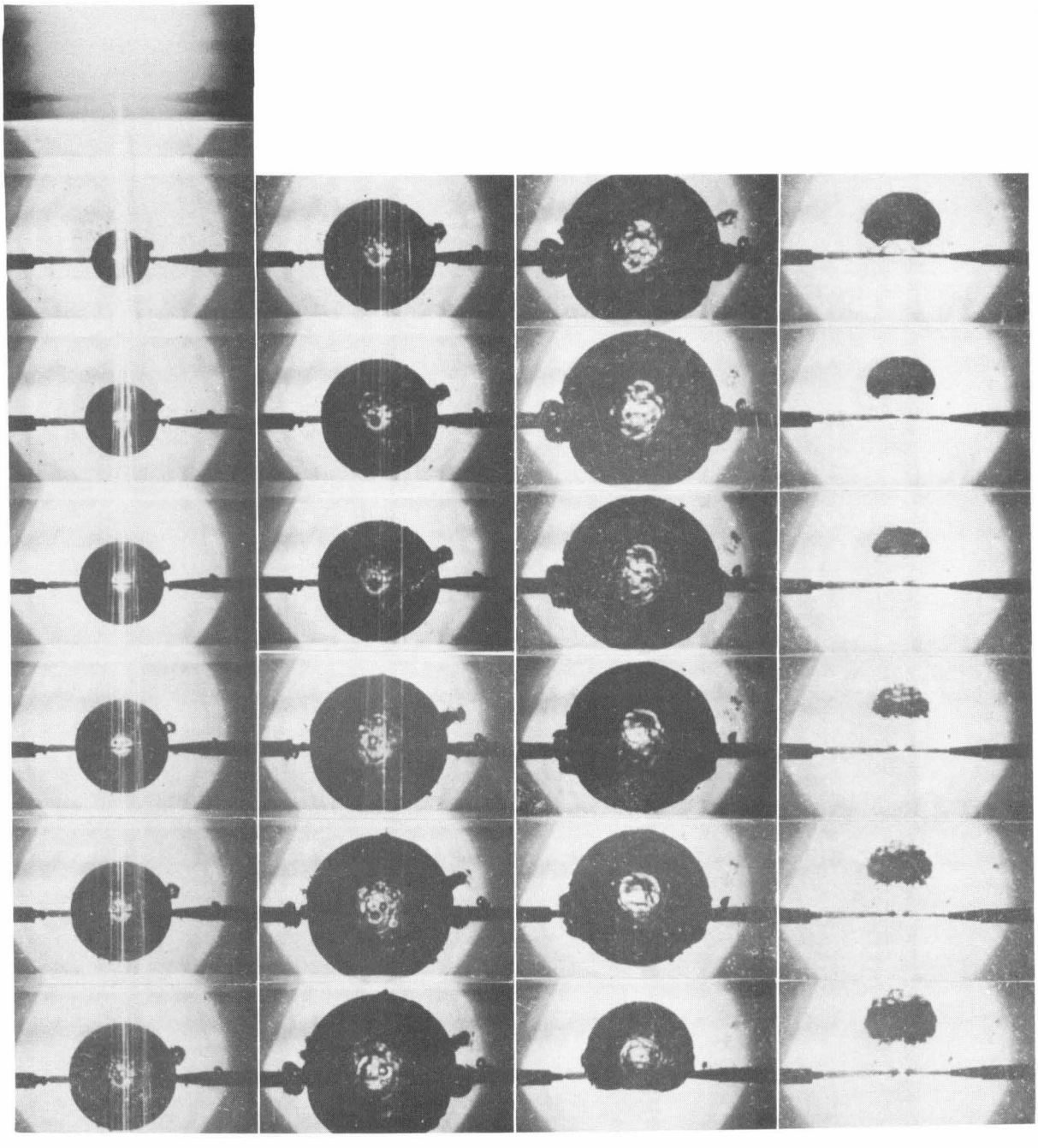

Fig. 26 - Collapsing spark bubble. Only every fifth frame is shown between frames 10 and 65. Frame 70 is the last one shown. $P - P_v = 0.55$ psia; Max. radius 1.62 in.; Collapse time 0.0223 sec.

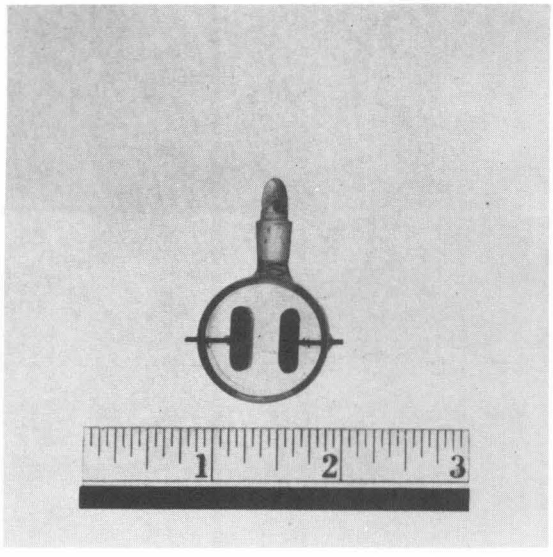

Fig. 27 - Kerr Cell.

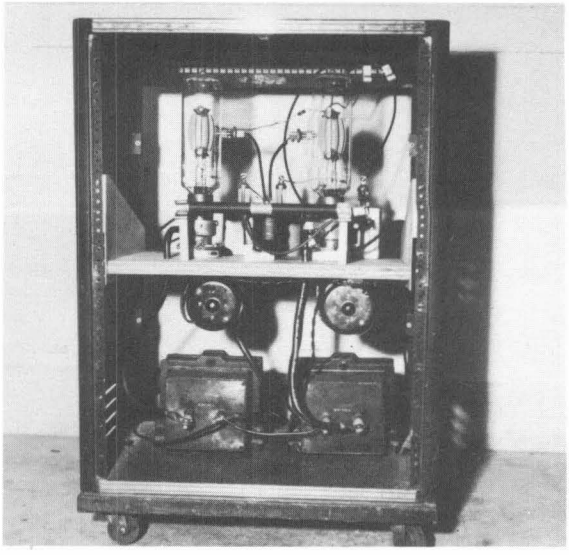

Fig. 28 - High level vacuum tube pulse amplifier.

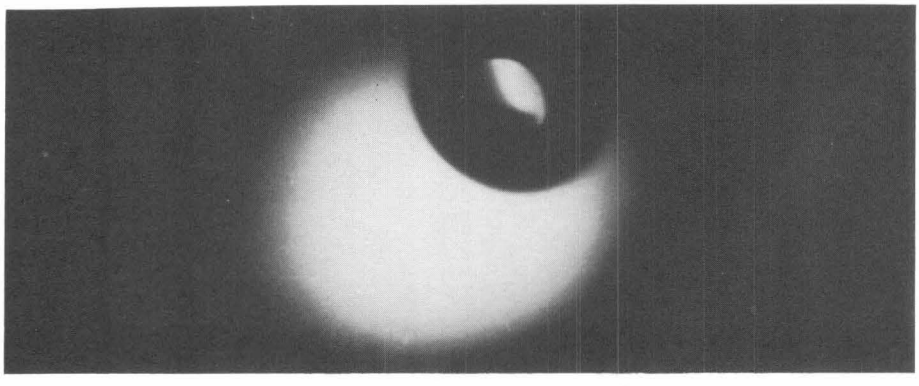

Fig. 29 - Bubble photograph taken with GE FT 231 Lamp.

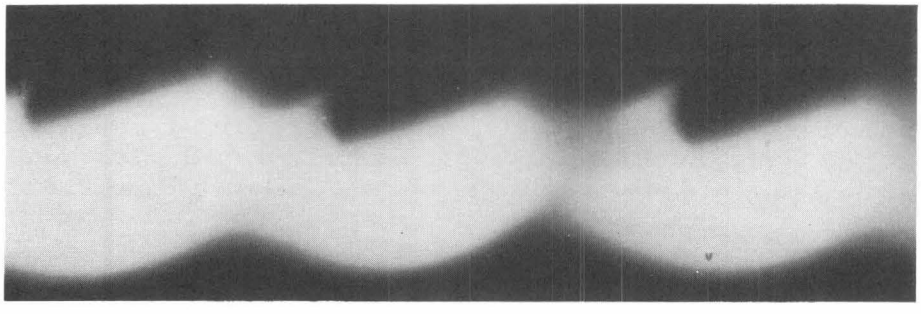

Fig. 30 - Solder bead photograph taken with GE FT 25 Lamp.

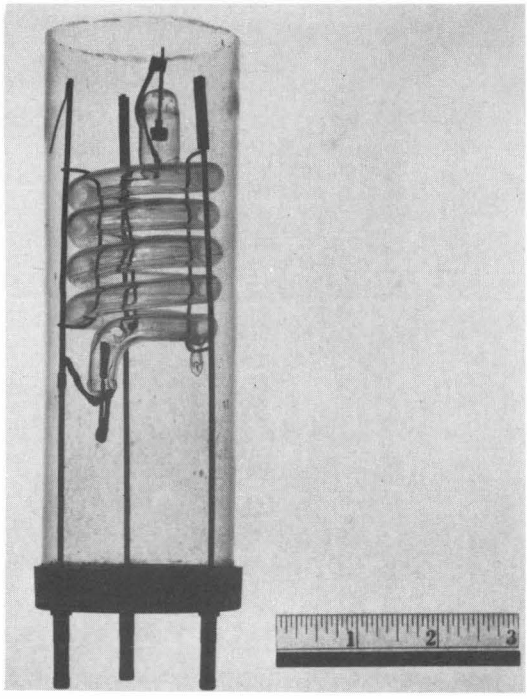

Fig. 31 - GE Flash Lamp.

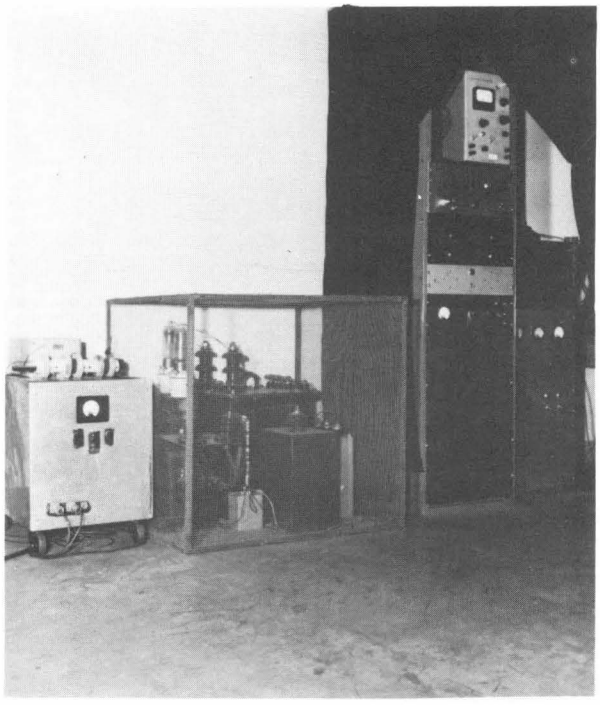

Fig. 32 - Electronic components of high-speed photography system.

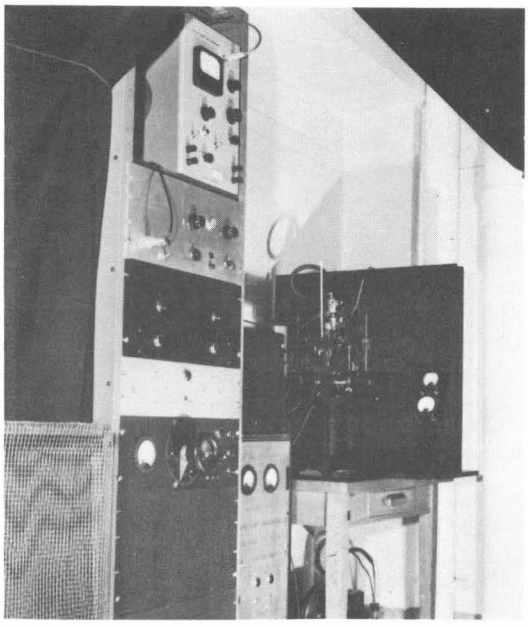

Fig. 33 - Pulser rack, power supply, camera and vacuum pump.

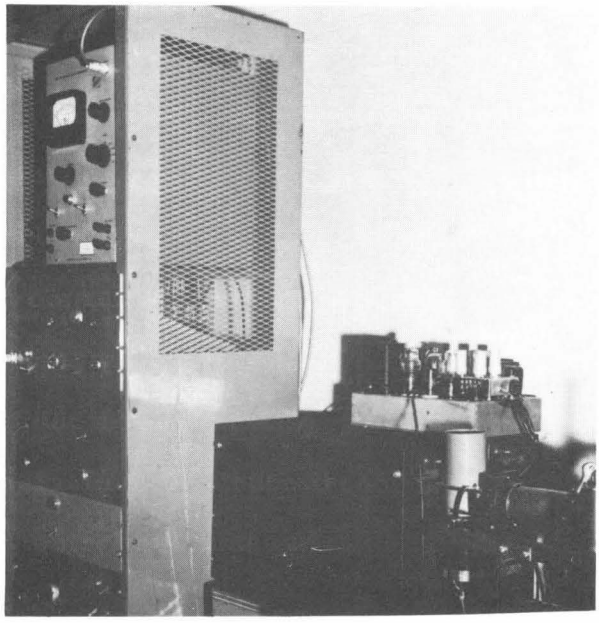

Fig. 34 - Bubble detector chassis resting on pulser with lamp housing in foreground.

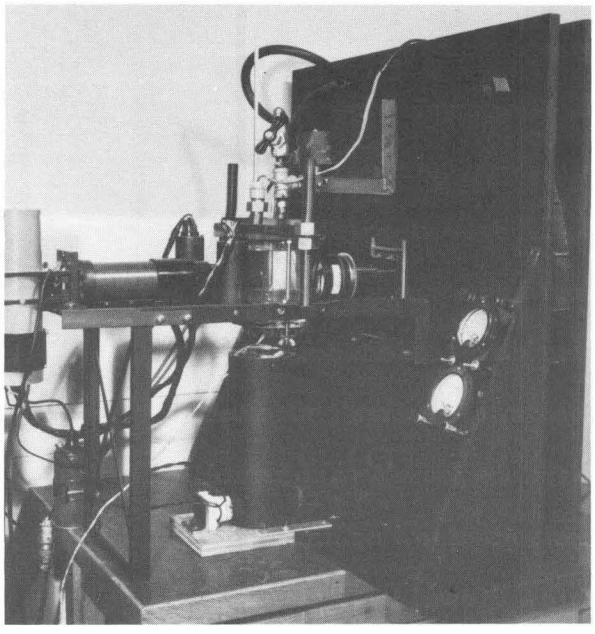

Fig. 35 - Rotating mirror camera, light source, and bubble collapsing equipment.

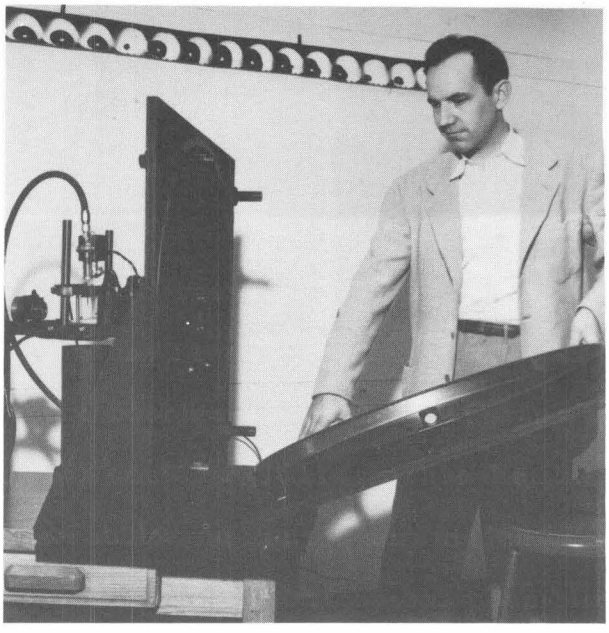

Fig. 36 - Side view of camera.

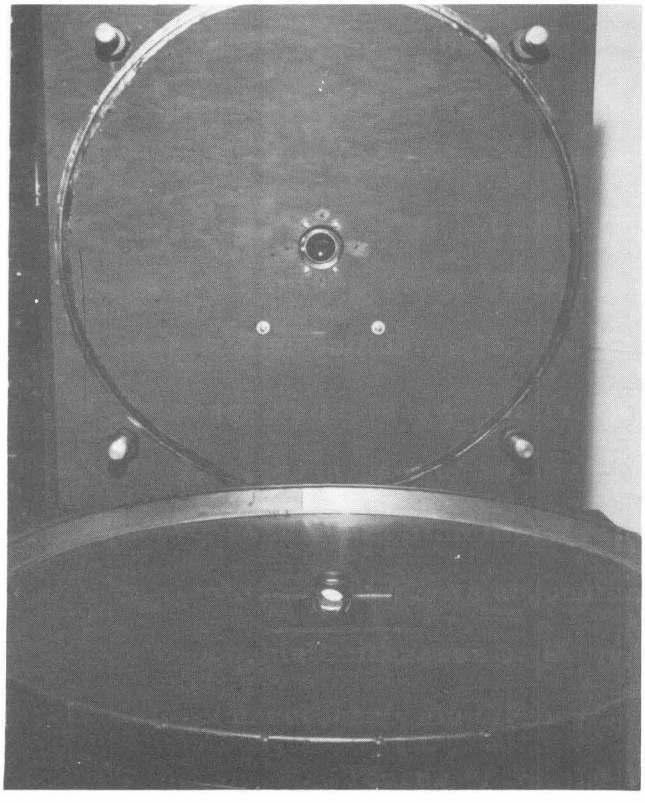

Fig. 37 - Rear view of camera showing film chamber open.

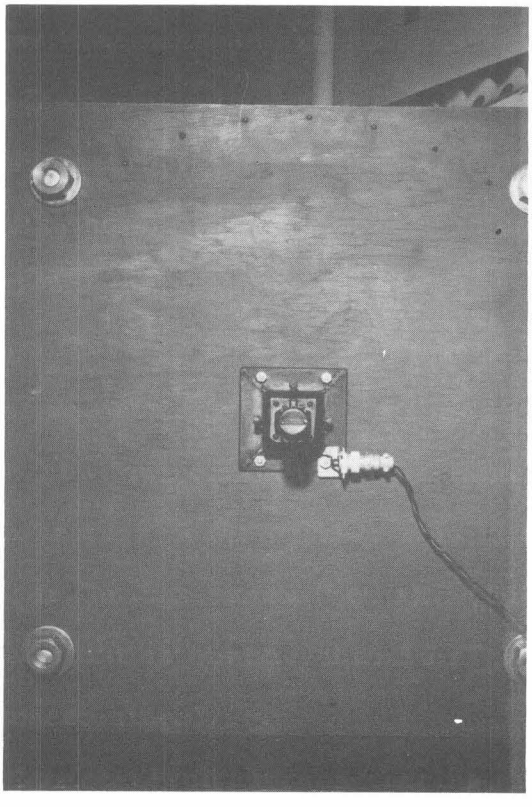

Fig. 38 - Rear view of camera showing mirror drive motor.

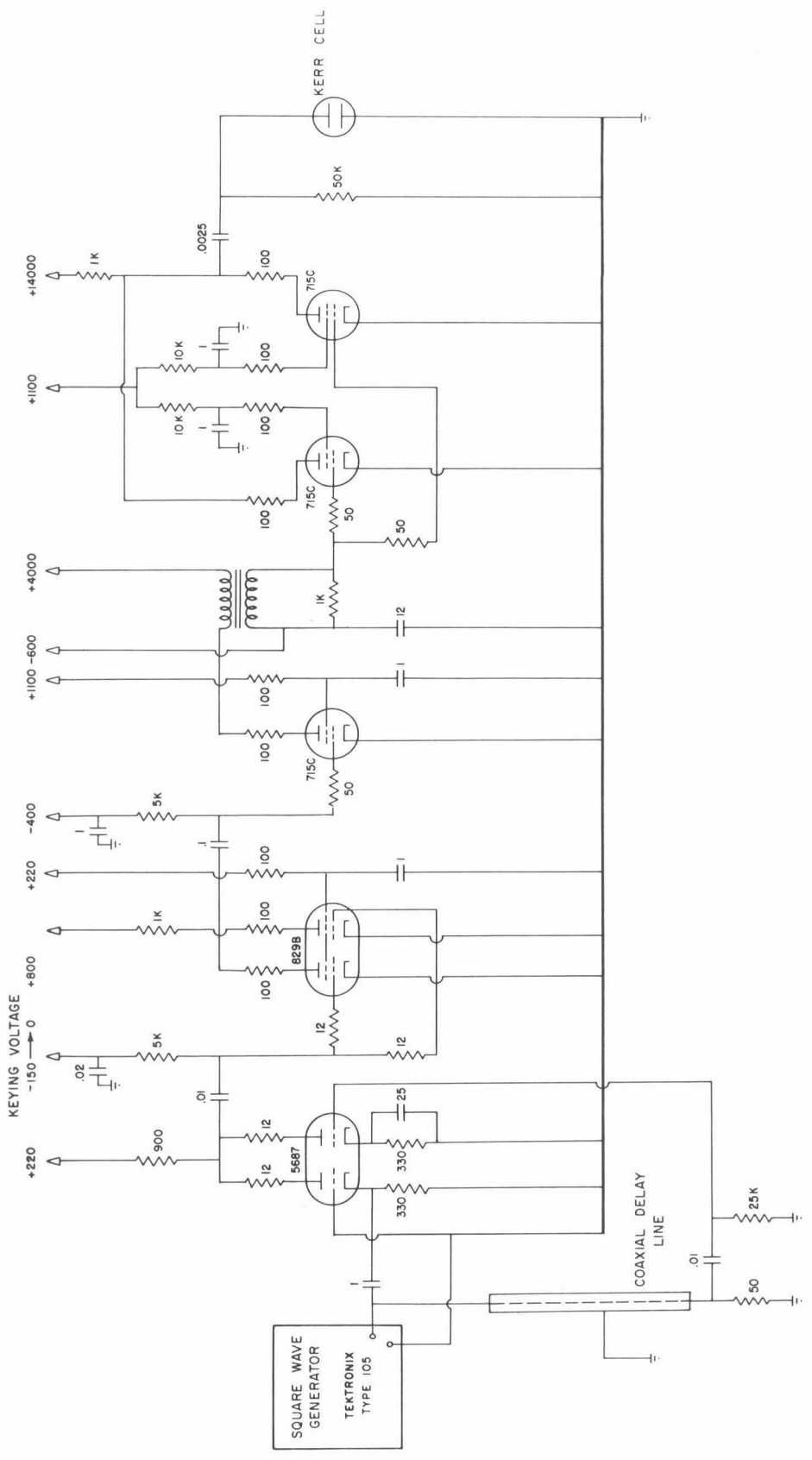

Fig. 39 - Kerr cell pulser wiring diagram.

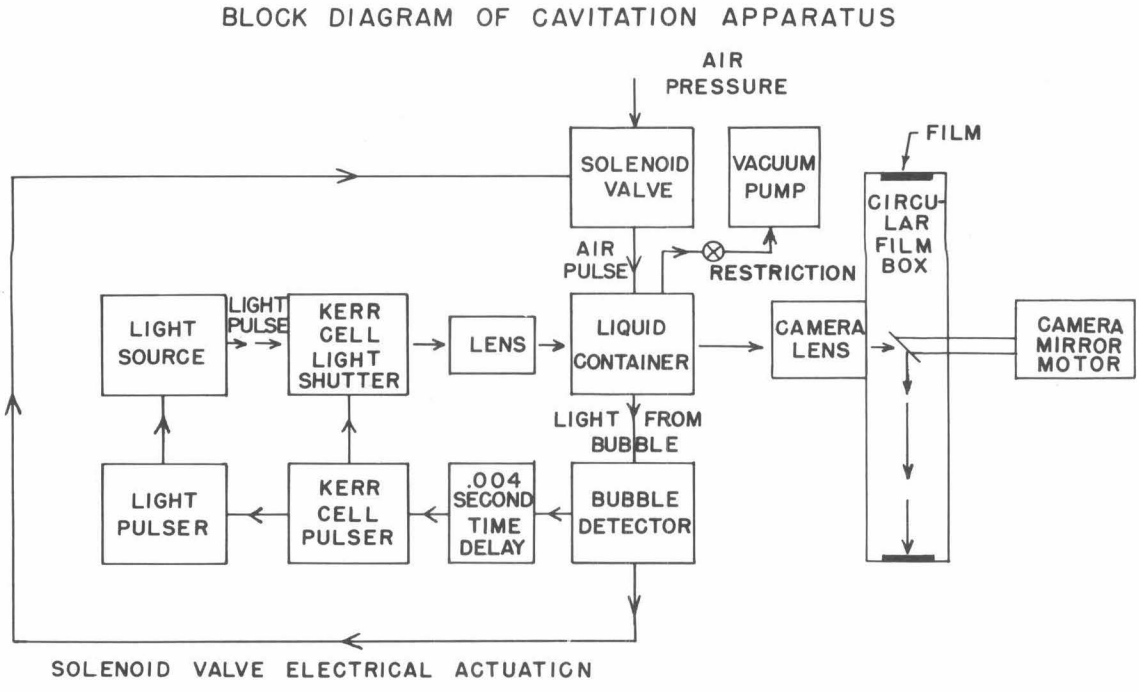

Fig. 40 - Block diagram of cavitation apparatus.

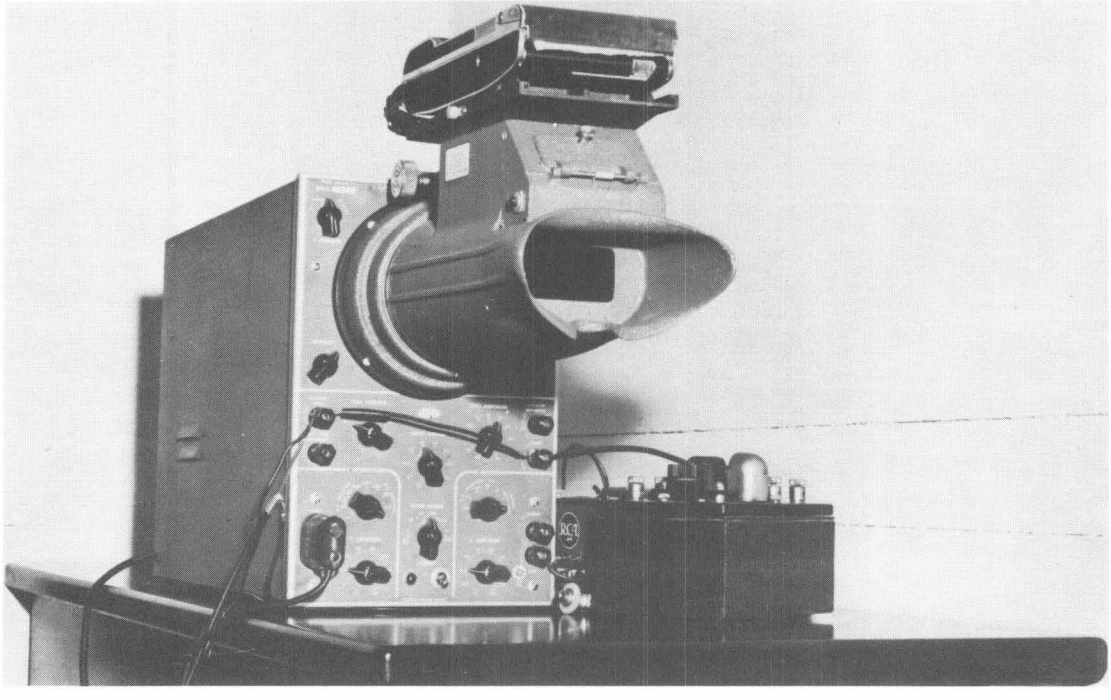

Fig. 41 - Pressure recording oscilloscope and camera with 1,000 cycle tuning fork.

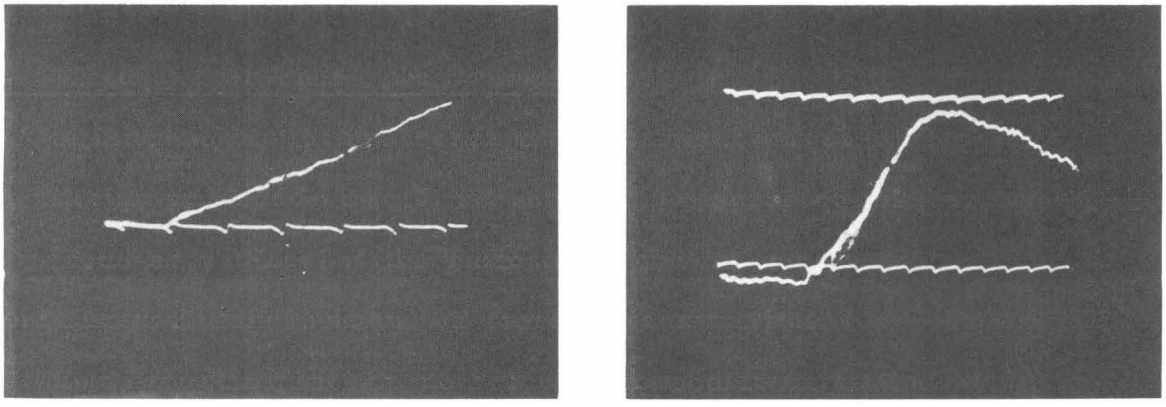

Fig. 42 - Sample pressure recorder.

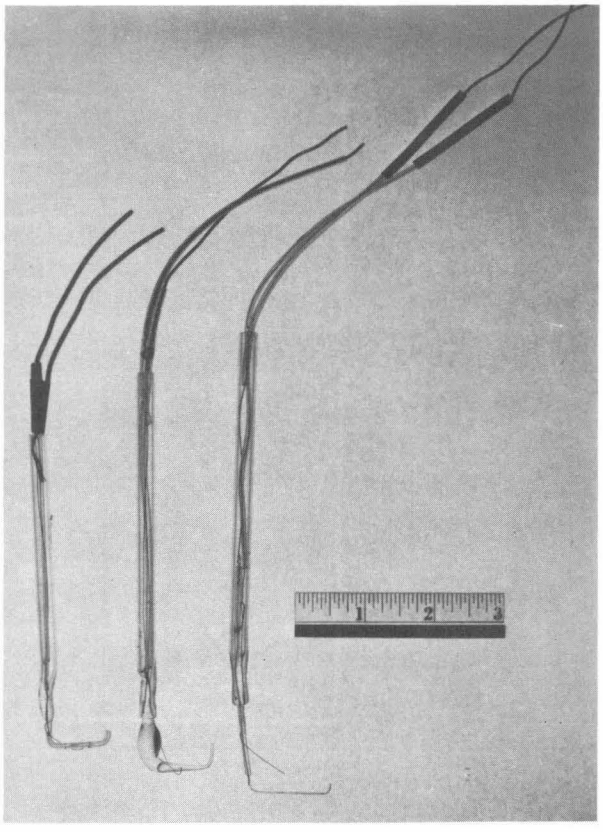

Fig. 43 - Bubble generators.

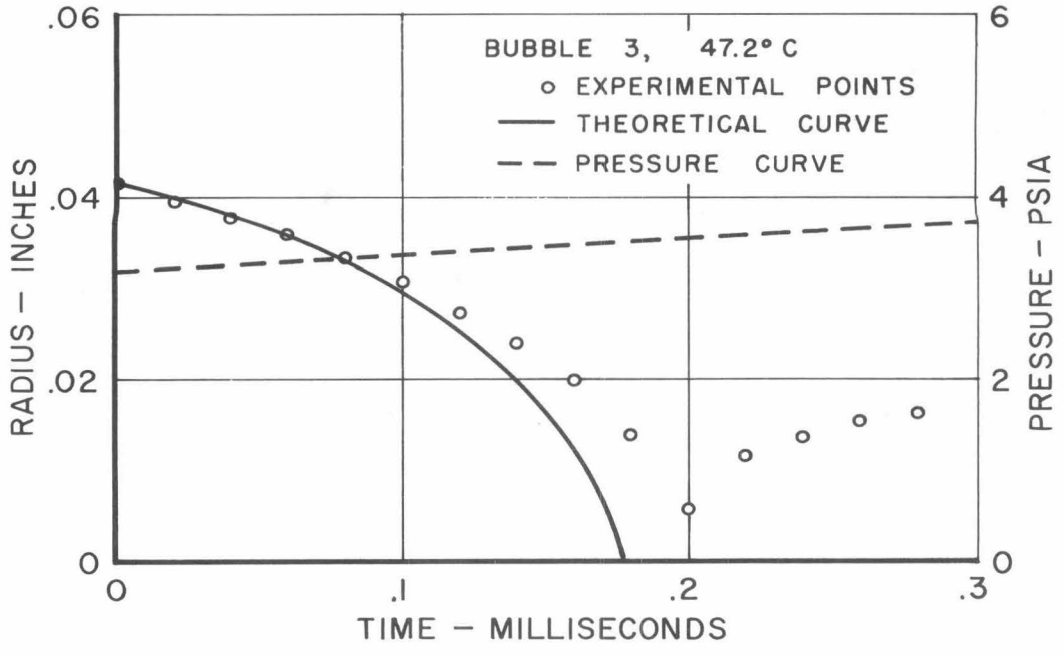

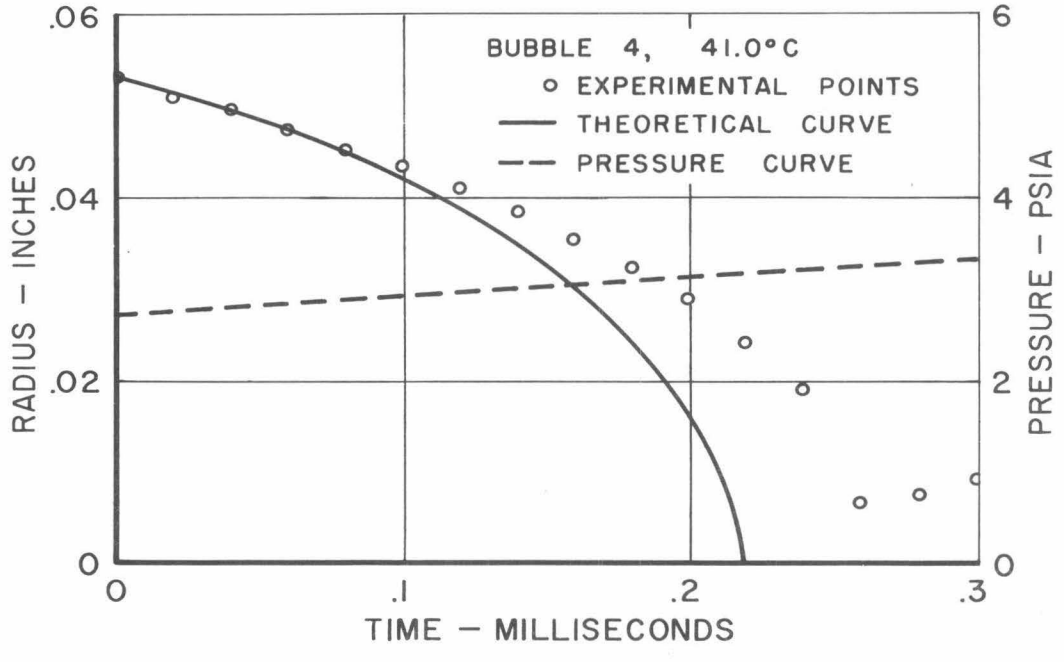

Fig. 44 - Bubble collapse in stationary liquid.

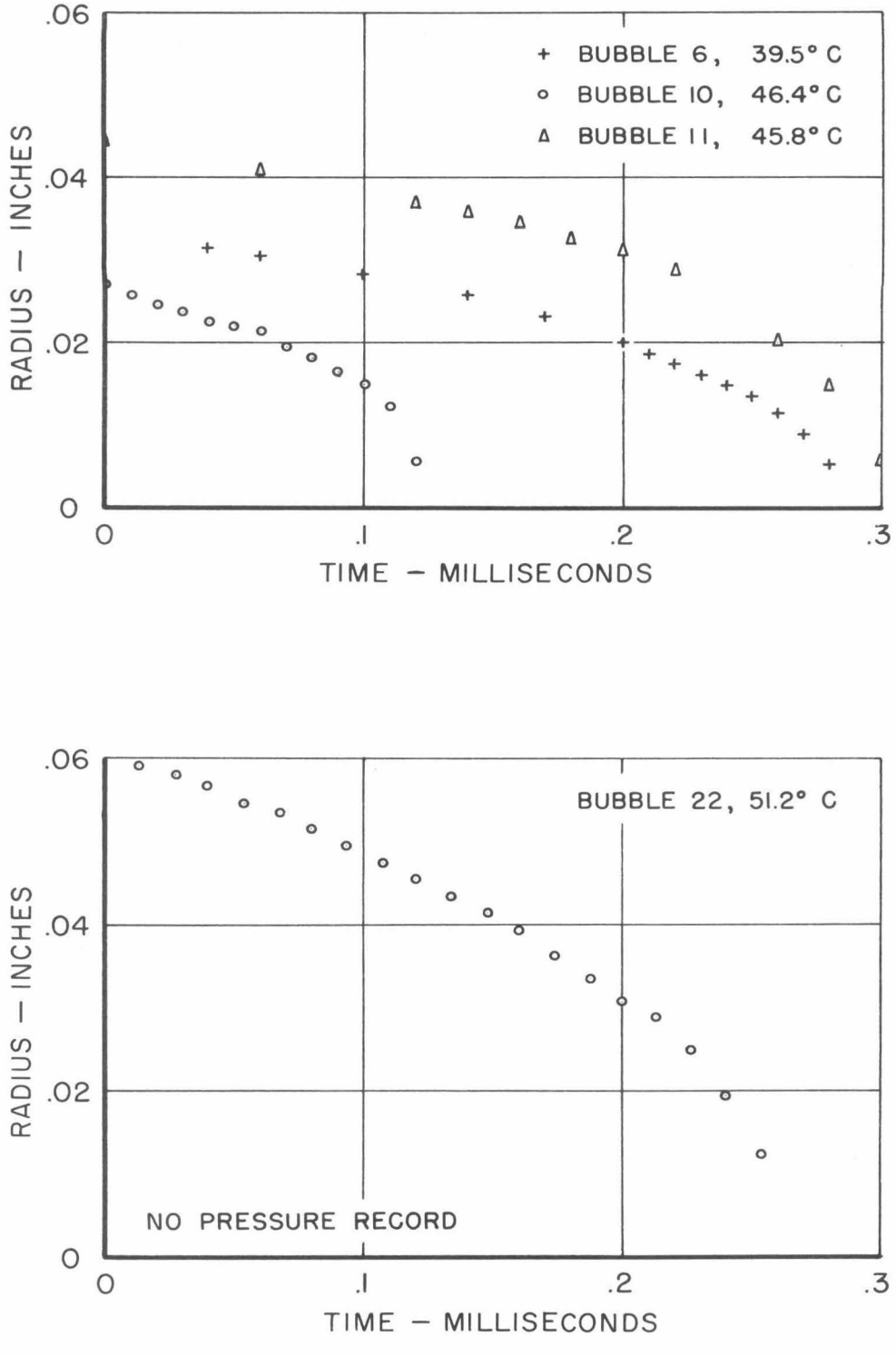

Fig. 45 - Bubble collapse in stationary liquid.

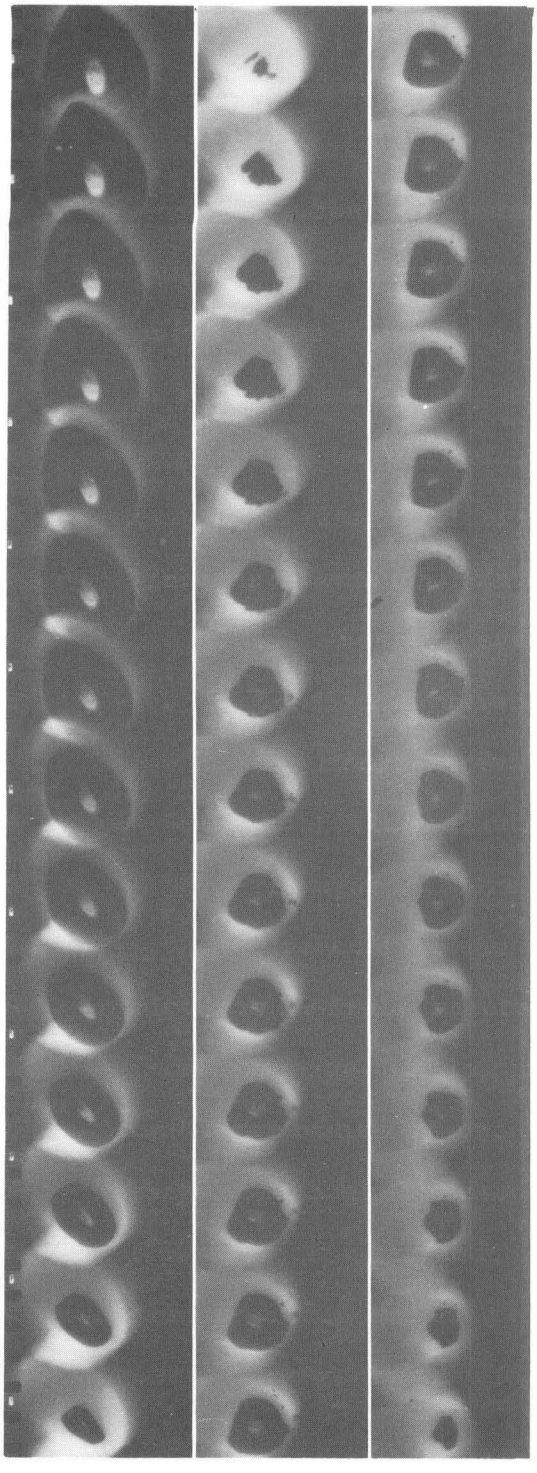

Fig. 46 - Bubble No. 3,
50,000 frames/sec.

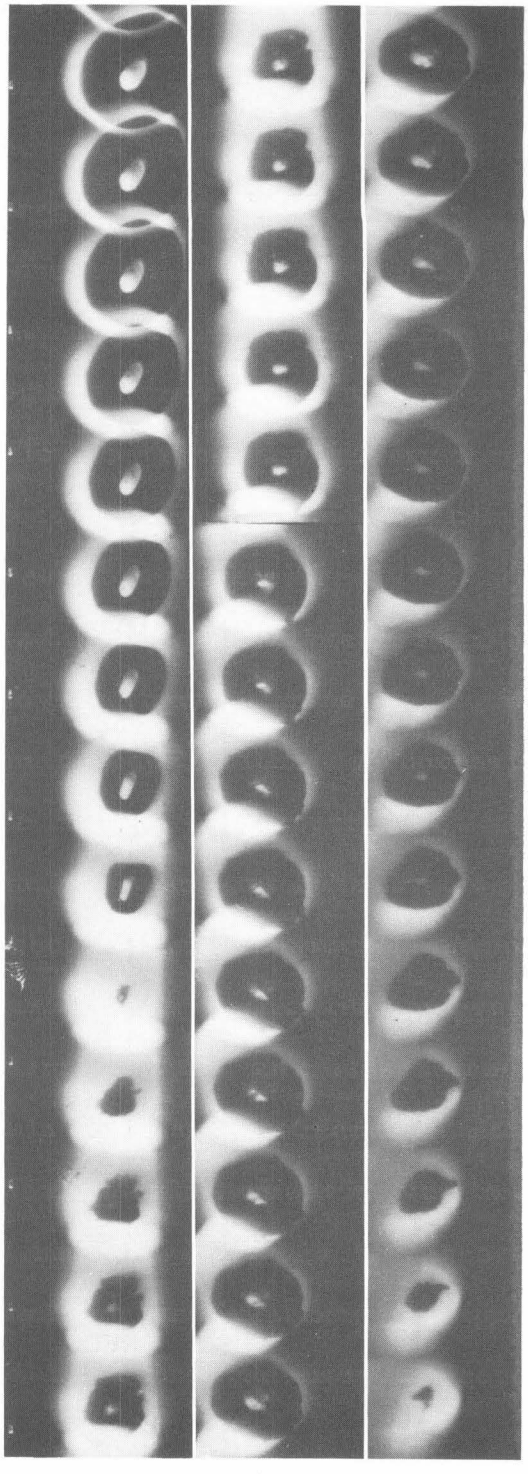

Fig. 47 - Bubble No. 4,
50,000 frames/sec.

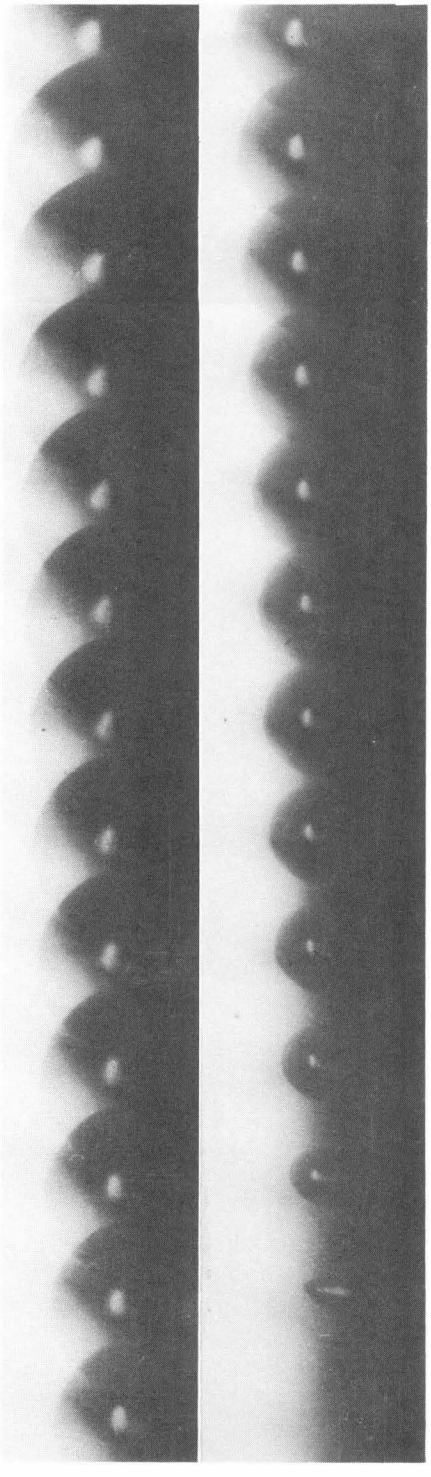

Fig. 48 - Bubble No. 6, 100,000 frames/sec.

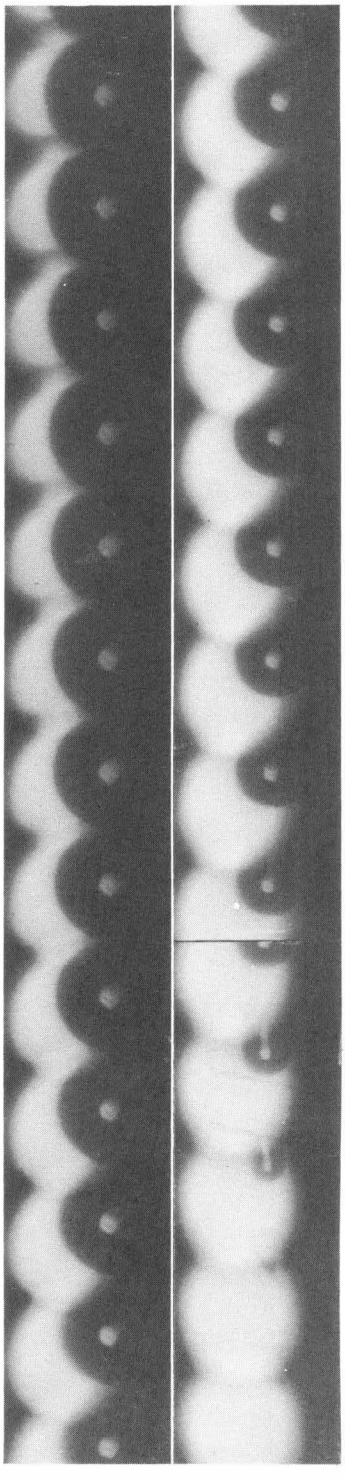

Fig. 49 - Bubble No. 11, 50,000 frames/sec.

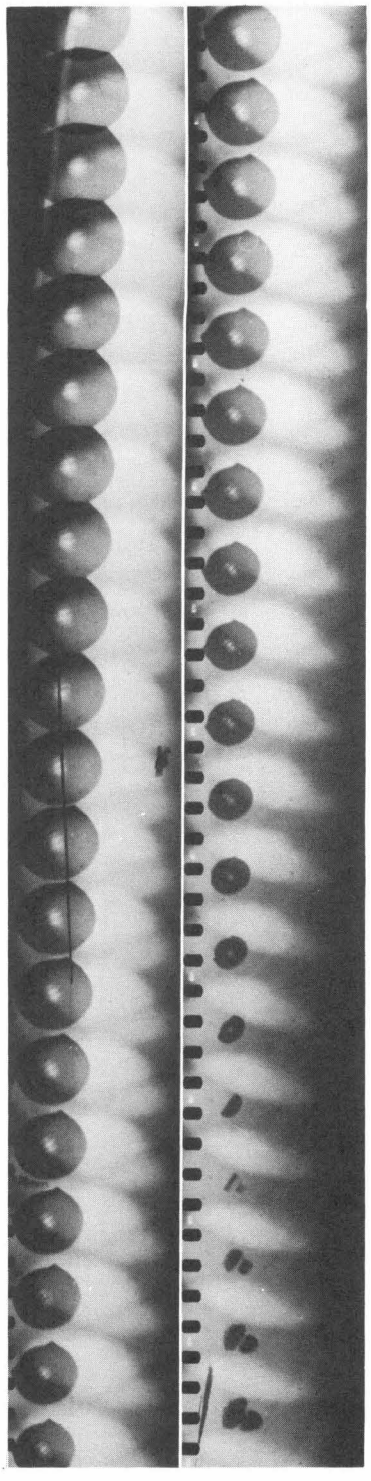

Fig. 50 - Bubble No. 22, 75,000 frames/sec.

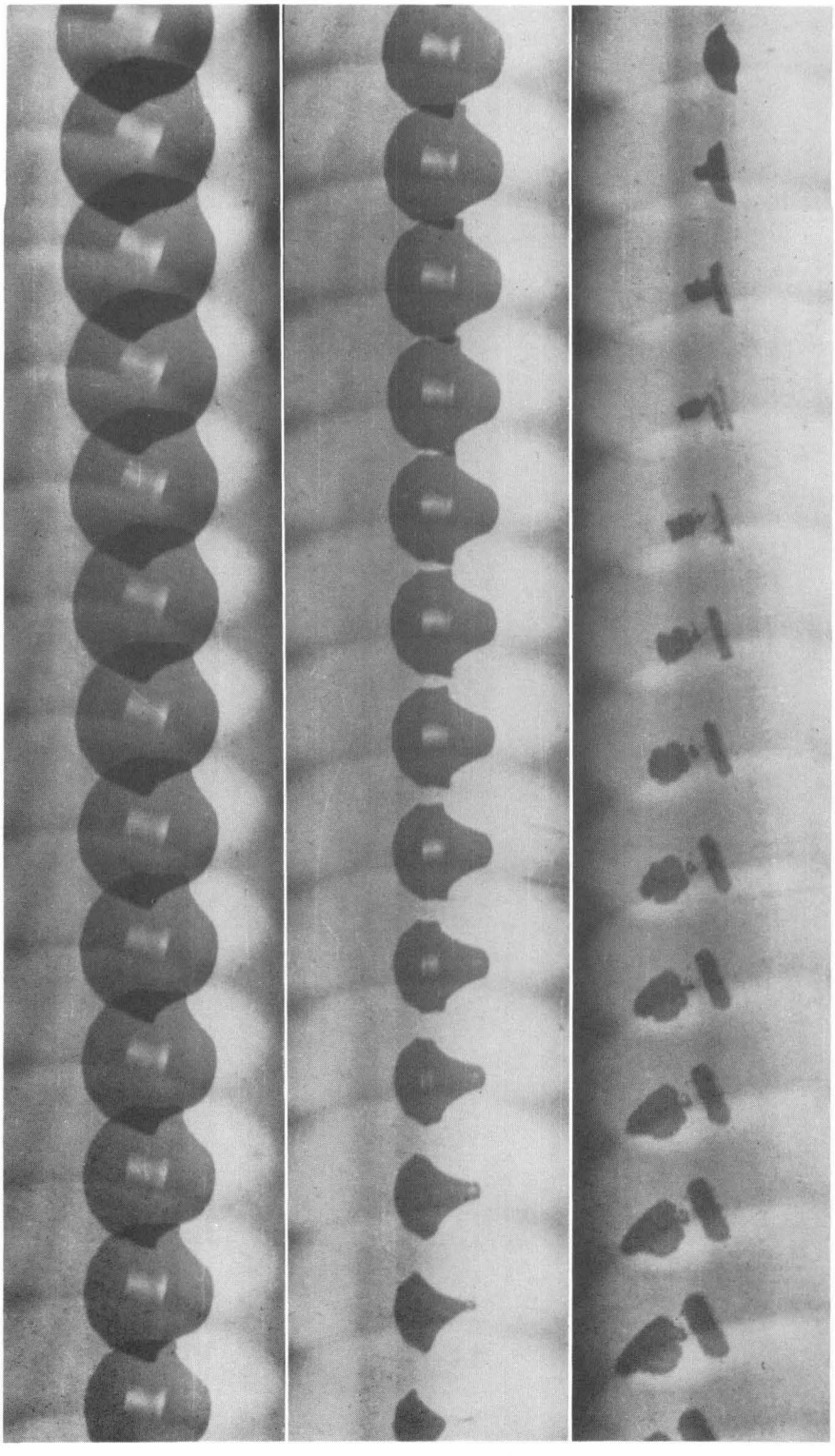

Fig. 51 - Bubble No. 24 - 100,000 frames/sec.

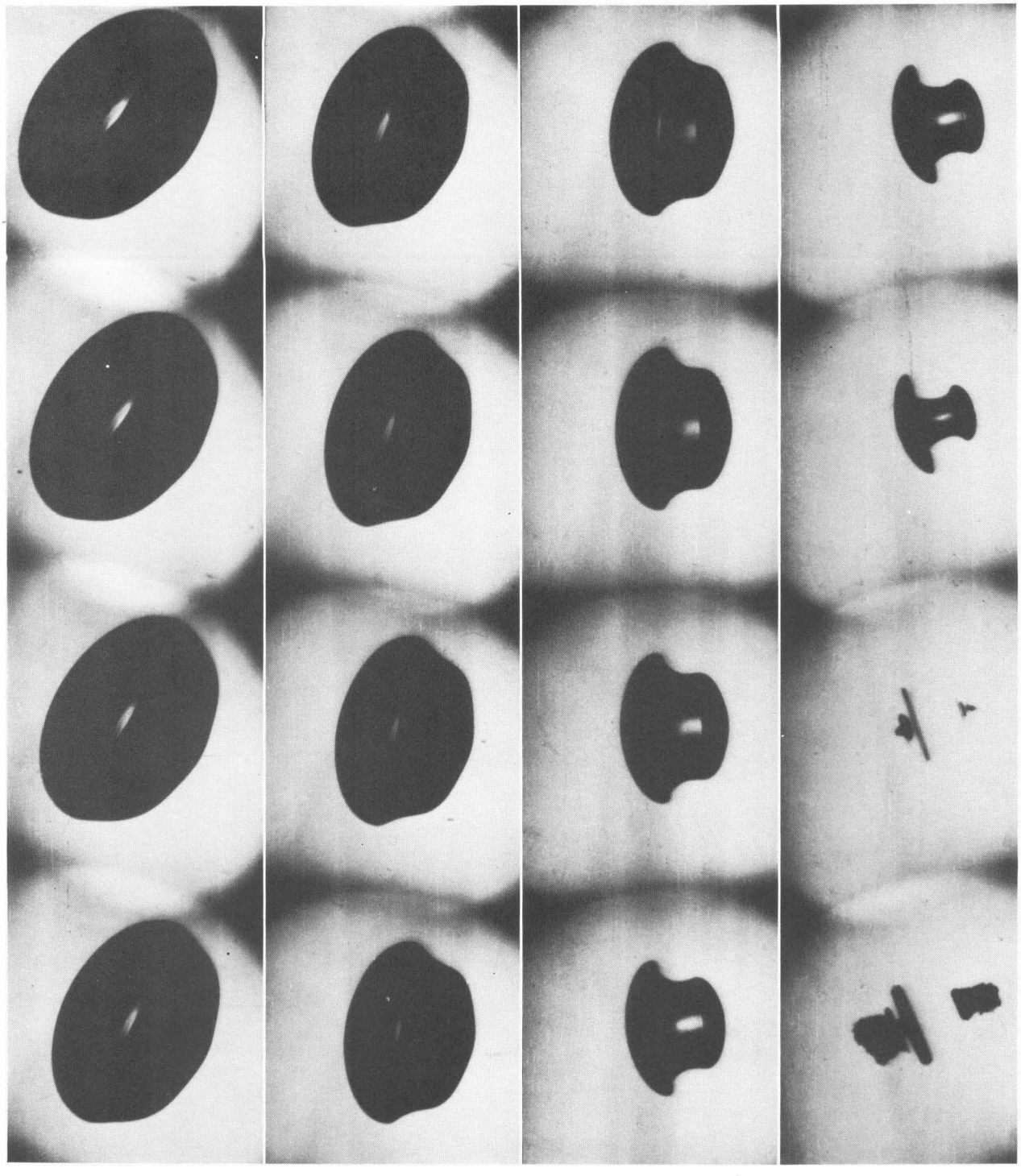

Fig. 52 - Bubble No. 21 - 33,000 frames/sec.

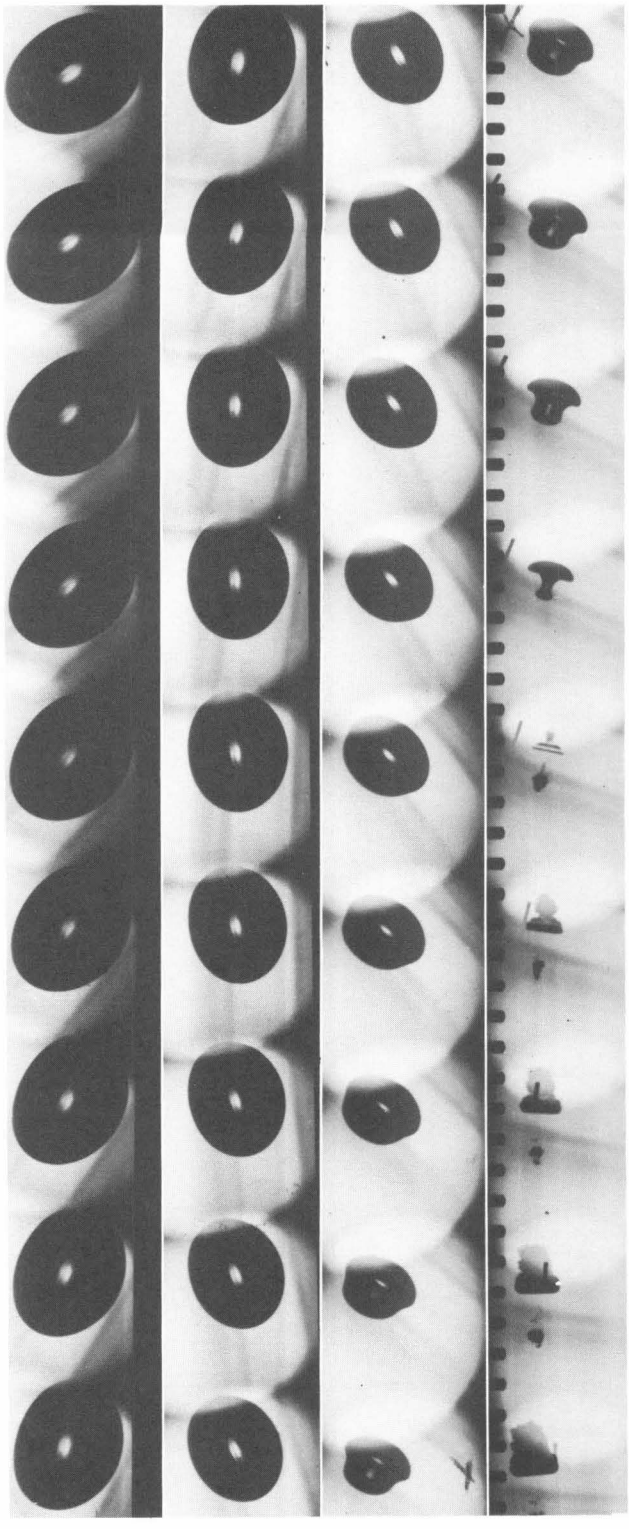

Fig. 53 - Bubble No. 29,
33,000 frames/sec.

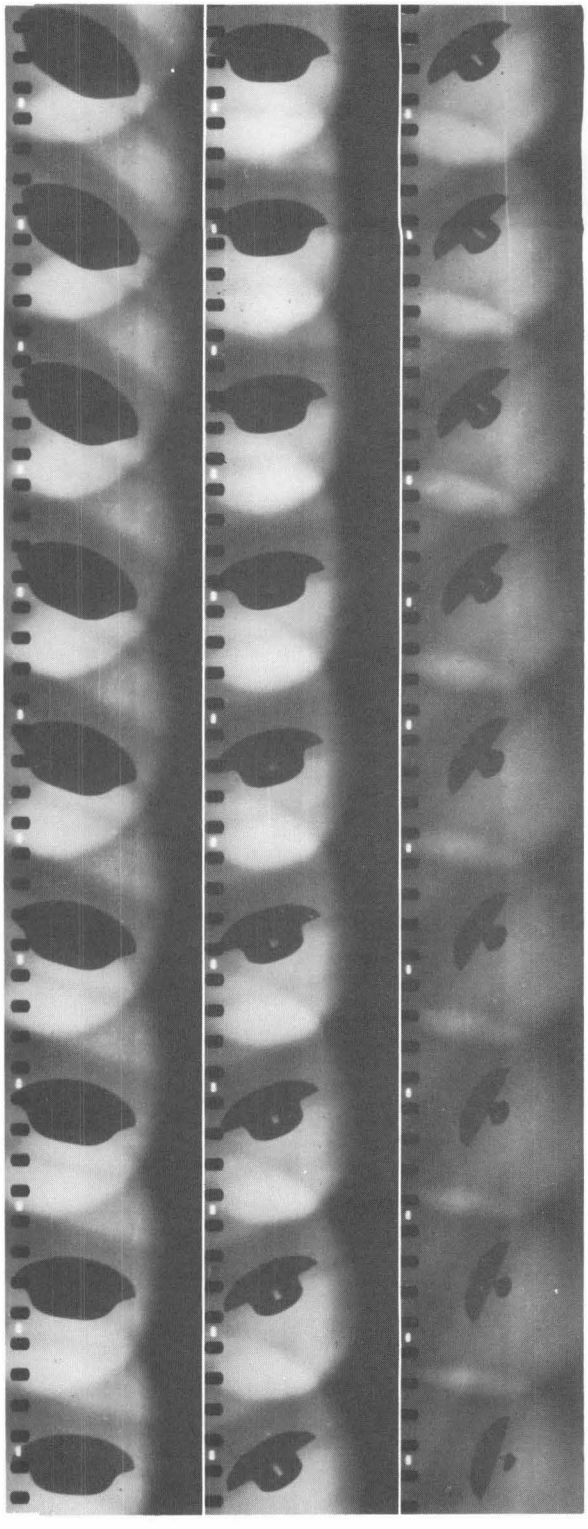

Fig. 54 - Bubble No. 50,
33,000 frames/sec.

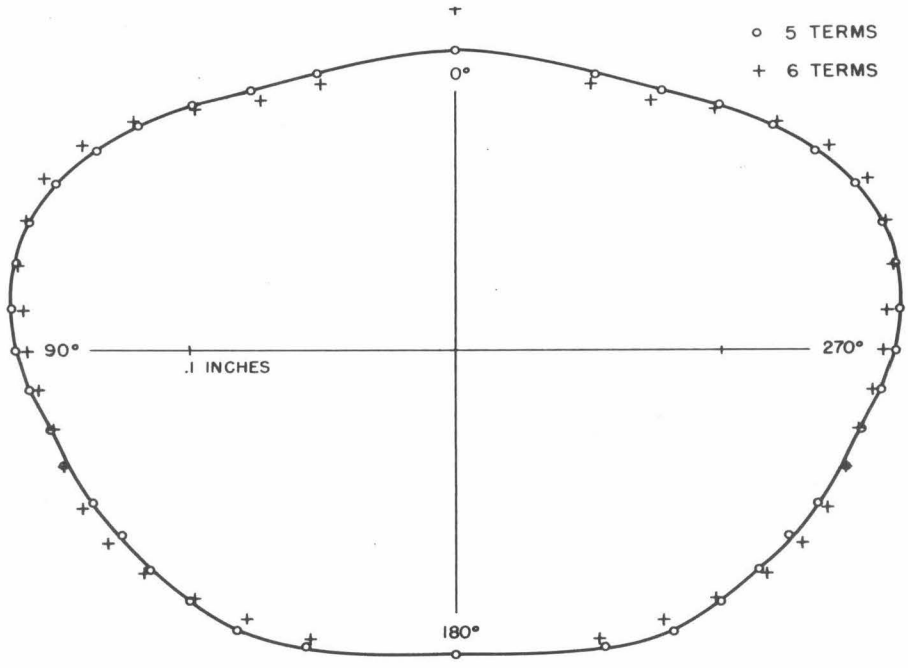

Fig. 55 - Synthesis of Bubble 21 from Legendre Polynomials.

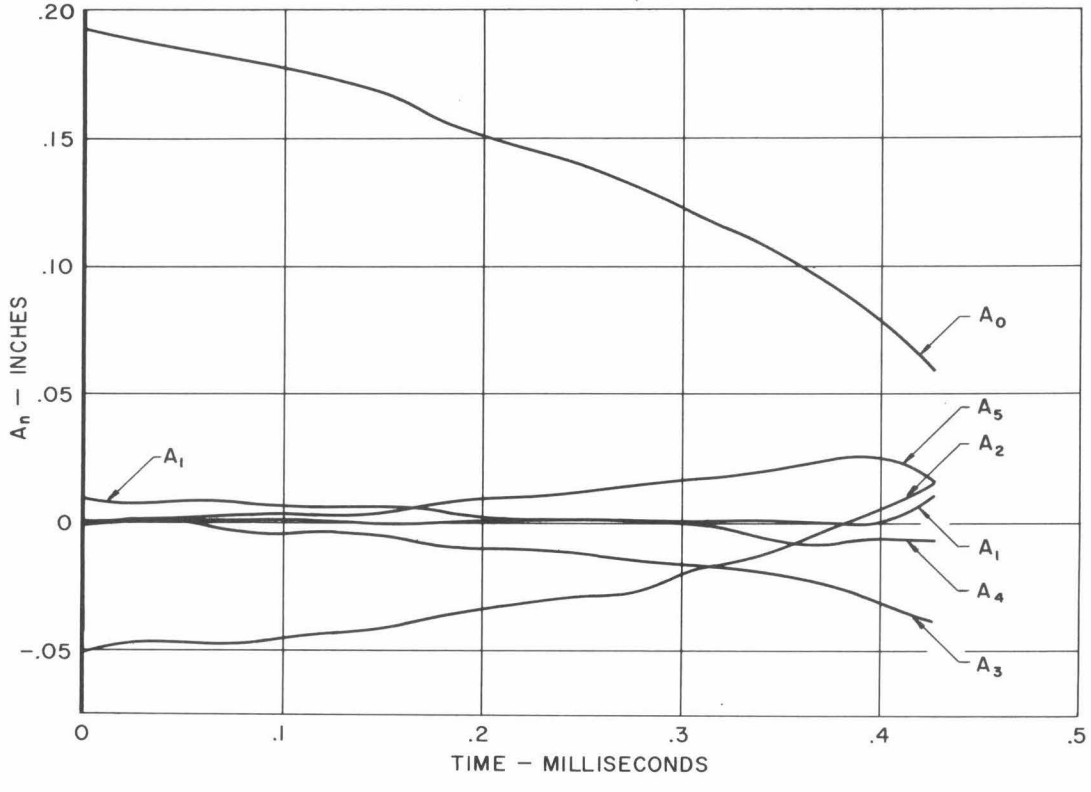

Fig. 56 - Variation of Legendre polynomial coefficients with time for Bubble 21.